

The Use of Quasi-Nonhydrostatic Models for Mesoscale Weather Prediction

A. E. MACDONALD

NOAA/ERL Forecast Systems Laboratory, Boulder, Colorado

J. L. LEE AND Y. XIE

*NOAA/ERL Forecast Systems Laboratory, Boulder, Colorado, and
CIRA, Colorado State University, Foothills Campus, Fort Collins, Colorado*

(Manuscript received 11 June 1998, in final form 19 August 1999)

ABSTRACT

In recent years, there has been extensive study of the mathematical basis of weather prediction leading to a new system of continuous equations that are well posed, and a set of conditions that make discrete atmospheric and other models stable and potentially more accurate. In particular, the theory deals with initial boundary value problems that admit multiple timescales. Using this theory, a quasi-nonhydrostatic model called QNH was developed at NOAA's Forecast Systems Laboratory. The model is fully compressible and explicit in the vertical as well as the horizontal direction. It is characterized by a parameter, " α " (typically the square of the vertical to horizontal aspect ratio), which multiplies the hydrostatic terms in the vertical equation of motion. In this paper, the authors describe the theoretical basis for the use of these models in mesoscale weather prediction. It is shown that for the mesoscale, the parameter has the effect of decreasing both the frequency and amplitude of the gravity wave perturbation response to small-scale impulses in forcing and to unbalanced initial conditions. This allows a modeler to choose a length scale below which gravity wave generation is suppressed. A weakness of the approach is that the hydrostatic adjustment process is slowed down. The analysis indicates that the parameter does not have an effect on the Rossby waves, the larger horizontal-scale gravity waves, nor on forced solutions such as those created by heating. The bounded derivative initialization is discussed. Since the speeds of the vertical acoustic waves are decreased, quasi-nonhydrostatic models can calculate the vertical equations explicitly and still meet the Courant–Friedrichs–Levy criteria. It is concluded that the unique characteristics of quasi-nonhydrostatic models may make them valuable in mesoscale weather prediction, particularly of clouds and precipitation.

1. Introduction

In recent years there has been extensive study of the mathematical basis of atmospheric, oceanic, and plasma models, leading to a theory of how to make their continuous equation systems well posed for the initial–boundary value problem (Kreiss 1980; Browning and Kreiss 1986). In particular, the theory addresses systems that admit multiple timescales. At National Oceanic and Atmospheric Administration (NOAA's) Forecast Systems Laboratory, a multiyear effort to apply the theory to mesoscale weather prediction has culminated in the development of a quasi-nonhydrostatic model called QNH, which will soon be used for real-time forecasting. In this paper, we discuss the theory and how it relates to mesoscale weather prediction. In another paper (Mac-

Donald et al. 2000), the design of the model and a test program are presented. A third related paper (Lee and MacDonald 2000) presents the initialization method prescribed by the theory and used in the model; the bounded derivative initialization.

While well-posedness applies to continuous equations, the application of the theory in numerical models leads to issues of stability. The concept of well-posedness of a continuous equation set, and the stability of a numerical model are closely related; in this paper, we present the theory mainly in terms of well posedness and then illustrate stability issues with the QNH model.

The well-posedness of hyperbolic systems was discussed by Kreiss (1970), while the issues associated with equations and models that admit multiple timescales were first outlined by Kreiss (1980). The scaling and conditions needed for implementation of a numerical model for weather prediction were presented by Browning and Kreiss (1986). Subsequent publications (Browning et al. 1989; Kreiss and Lorenz 1989; Browning and Kreiss 1994a, 1997) have extended the theory and further described its characteristics and use. The

Corresponding author address: A. E. Macdonald, NOAA/ERL Forecast Systems Laboratory, R/E/FS, 325 Broadway, Boulder, CO 80303.
E-mail: macdonald@fsl.noaa.gov

type of model that is described in this paper was referred to by Browning and Kreiss (1986) as the “approximate system” and has been referred to more recently as the “multiscale system” (Browning and Kreiss 1994a). It is characterized by a parameter in front of the hydrostatic term of the vertical equation of motion, with the value of the parameter typically chosen as the square of the vertical to horizontal length scale (the aspect ratio) of the smallest phenomenon of interest. The parameter can be assigned a value between limiting cases near 0, where the model is very stable, and 1, which is purely nonhydrostatic. We refer to this type of model as “quasi-nonhydrostatic,” encompassing a range of parameters and associated model behavior that will be described in the paper.

Although the mathematical theory associated with quasi-nonhydrostatic models has been well developed, it has not been investigated or tested significantly in association with the physics (e.g., moisture, turbulence, radiation) required for weather prediction. This paper discusses the advantages and disadvantages in the application of these models to mesoscale weather prediction and, in particular, clarifies the effect of the quasi-nonhydrostatic constant on small-scale gravity waves. It is shown that the constant decreases the frequency and amplitude of gravity waves generated by forcing, which is small in the horizontal scale, but deep in the vertical scale.

The primary advantage of quasi-nonhydrostatic models is related to their well-posedness (continuous equations) and for numerical prediction, the stability associated with the suppression of generation of small-scale gravity waves. The theory for nearly symmetric, hyperbolic systems prescribes conditions needed to ensure existence of a solution for a period of time, which means that excessive sensitivity to errors in numerical approximations, small-scale perturbations of initial conditions and forcing are limited. In short, it allows the modeler to choose the scales and phenomena of interest, and ensures a stable integration of the system through a forecast period. This is in contrast to hydrostatic models with pointwise boundary conditions that have been shown to be ill posed (Oliger and Sundstrom 1978); furthermore, it has been shown that hydrostatic models are unstable for small-scale moist processes (Orlanski 1981). Pure nonhydrostatic models can be made well-posed; however, common practices such as the use of semi-implicit and split-explicit schemes may result in unstable models (Browning and Kreiss 1994b), often ameliorated by some combination of implicit and explicit smoothing. If a particular phenomenon is the target of a prediction model [e.g., cloud and precipitation for the $O(100\text{-km})$ scale], then proper choice of the quasi-nonhydrostatic parameter will result in a more stable model integration because of reduced energy in the high-frequency waves.

A disadvantage of quasi-nonhydrostatic models is due to their slower adjustment to hydrostatic equilib-

rium. The smaller the constant, the slower the model will adjust. Thus quasi-nonhydrostatic models and nonhydrostatic models differ in their approximations. The issue of which of these results in better weather forecasts for a particular phenomenon (e.g., precipitation or downslope windstorms) is empirical. Only extensive experience can show which is better for each phenomenon.

The main goal of the quasi-nonhydrostatic model development at Forecast Systems Laboratory (FSL) has been short-range mesobeta-scale (order 100 km, as defined by Orlanski 1975) weather prediction, with particular emphasis on cloud and precipitation. Despite great economic importance, the ability to forecast heavy precipitation has been low, and although some progress has been made (Black et al. 1990), much room for improvement remains. The QNH model has generally been tested at horizontal grid meshes between 5 and 20 km (MacDonald et al. 2000), which are the target resolutions for the weather prediction model during the next several years. It is shown in section 2 that several of the characteristics of quasi-nonhydrostatic models are helpful for the short-range, limited-domain models that are commonly used in mesoscale weather prediction. The bounded derivative initialization technique, described in section 2d and detailed in Lee and MacDonald (2000), allows a smooth and accurate model integration from the initial time, without the a period of adjustment or model shock common in limited-area models. Furthermore, the bounded derivative initialization should allow a “hot start” model, with latent heating and precipitation existing and accurately balanced and predicted from the initial time. A well-posed boundary is described in section 2e that allows acoustic, gravity, and Rossby waves to enter and exit smoothly through the boundaries of a limited domain. This is an advantage for small domains and also an advantage for nesting of higher resolution grids, since the lateral boundary problems are significantly reduced. The combined advantages of bounded derivative initialization and well-posed boundaries offer the potential for very short-range (a few hours), small-domain predictions.

One effect of the quasi-nonhydrostatic parameter is to slow down the speed of the vertical acoustic waves, as shown in section 2g. (Among other effects, this slows down the model’s adjustment to hydrostatic equilibrium.) The time needed for an acoustic wave to cross a grid cell can be made the same in the horizontal and vertical directions. This suggests the use of explicit calculations in the vertical, since the Courant–Friedrichs–Levy (CFL) required time step needed for the vertical calculation is the same as that for the horizontal. This has two important implications. First, it allowed the design of the QNH model to be simplified, since the horizontal is treated similarly to the vertical; as discussed in MacDonald et al. (2000), fourth-order space differencing was used in all space calculations,

which resulted in highly accurate treatment of the vertical dynamics. A second implication is that the model is unique in its treatment of the vertical coordinate for mesobeta scales, where most modelers are using implicit formulations.

An important aspect of the quasi-nonhydrostatic type of model is related to how they accommodate gravity waves. The results of an extensive analysis of various atmospheric waves is given in section 3. It is shown that the quasi-nonhydrostatic parameter, α , does not affect the Rossby waves, nor the forced waves, such as those created by adjustment to heating. Thus, an important difference between a quasi-nonhydrostatic model ($\alpha < 1$) and a fully nonhydrostatic model ($\alpha = 1$) is in how the gravity waves are modified. Both the linear analysis and experiments with the model indicate that the response of the model to impulses in forcing such as heating, is to decrease the frequency and amplitude of the smaller-scale gravity waves compared to those in a fully nonhydrostatic model. The amount of the decrease is shown to depend on the constant α , and on the vertical and horizontal wavelength of the gravity wave. The modeler chooses, by the choice of α , the scales (larger) of the gravity waves that will respond fully to impulses, and equivalently, the scales (smaller) that will intentionally have decreased response to impulses. The analysis of Browning and Kreiss (1997) indicates that small-scale gravity waves should have comparatively small amounts of energy, which suggests that the alteration of such waves by numerical methods (e.g., the use of α or semi-implicit techniques) is acceptable.

It has been pointed out that the parameter α particularly affects the terrain-forced gravity waves (Skamarock and Klemp 1994), with a potential for improper ducting. An analysis of this difficulty and an example of its effect on the model's simulation of Long's (1953) solution of mountain waves is given in section 3b. The example shows that such improper ducting can indeed occur. However, gravity waves of any scale can be accommodated within the QNH model by appropriate choice of α . Once a particular choice is made, such as $\alpha = 10^{-2}$, terrain scales that are significantly smaller can and should be eliminated from the bottom boundary condition.

2. Theory and description

a. Dynamic equations

The dynamic equations are formulated similar to Browning and Kreiss (1986) with the exception that perturbation potential temperature, rather than its inverse, is used:

$$\frac{du}{dt} = -\frac{1}{\rho_0} \frac{\partial p}{\partial x} + fv \quad (1)$$

$$\frac{dv}{dt} = -\frac{1}{\rho_0} \frac{\partial p}{\partial y} - fu \quad (2)$$

$$\frac{dw}{dt} = \alpha \left[-\frac{1}{\rho_0} \frac{\partial p}{\partial z} + g\theta - \frac{g}{\gamma P_0} p \right] \quad (3)$$

$$\frac{dp}{dt} = -\gamma P_0 \left(\frac{\partial u}{\partial x} + \frac{\partial v}{\partial y} + \frac{\partial w}{\partial z} \right) + \rho_0 gw \quad (4)$$

$$\frac{d\theta}{dt} = -\tilde{\theta}w, \quad (5)$$

where u , v , and w are the x , y , and z components of wind velocity; p is the perturbation pressure; and θ is the perturbation potential temperature defined by

$$\theta = \frac{\theta_{\text{total}}}{\theta(z)} - 1.$$

The quasi-nonhydrostatic parameter, α , is typically taken as the square of the aspect ratio,

$$\alpha = (\Delta z / \Delta x)^2.$$

The constants γP_0 and $\tilde{\theta}$ are given by

$$\gamma P_0 = 1.4 \times 10^5 \quad \tilde{\theta} = \frac{1}{\theta(z)} \frac{\partial \theta}{\partial z}.$$

The total derivative is given by

$$\frac{d}{dt} = \frac{\partial}{\partial t} + u \frac{\partial}{\partial x} + v \frac{\partial}{\partial y} + w \frac{\partial}{\partial z}.$$

This set of five prognostic equations with five unknowns is derived from the conservation relations for momentum, mass, and thermodynamic energy. Density has been eliminated from the prognostic set by use of the equation of state, and appears in the prognostic set as ρ_0 , a function of z , which is constant in time. When the system is analyzed as shown in appendix A, a characteristic equation with five roots is obtained. Two of the roots are acoustic waves, two are gravity waves, and the last is the Rossby wave.

The dynamic formulation is very similar to that used in many atmospheric models, with the exception of the parameter, α , which will be discussed in section 2c. In the derivation of the equations, the hydrostatic balance of the mean state has been subtracted off. The net result of the use of variables, which are deviations from the mean, is that the numerical accuracy of the system is enhanced (Browning and MacDonald 1993). Three other approximations deserve mention. First, ρ_0 rather than the fully variable density is used. Second, the velocity form rather than the flux form of the momentum equations is used. Third, the last term in (3) makes the set more symmetric, being adjoint to the last term in (4).

These approximations are discussed in Browning and Kreiss (1986).

b. Multiple timescales, symmetry, and well posedness

Kreiss (1980) has developed a theory for symmetric hyperbolic partial differential equations that admit waves with different timescales. In weather prediction, the acoustic waves are clearly fast waves, while the Rossby waves are slow; the theory deals with “stiff” systems that admit these two widely different timescales, as well as the gravity waves that are intermediate. The theory is elaborated and detailed for multiple timescales in Browning and Kreiss (1986), Browning and Kreiss (1994a), and Browning and Kreiss (1997). Kreiss and Lorenz (1989) discuss concepts of well-posedness for Navier–Stokes and related equation systems. Mathematically, a problem is well posed if its solution exists, is unique, and depends continuously on the data. In practical terms, the theory shows how solutions respond to small changes in initial conditions, boundary conditions, and physical forcing. This is especially important in mesoscale prediction, since forcing such as latent heating can be quite strong and “rough.” The concept of roughness is related to large gradients in time and space, which violate the smoothness assumptions needed in proofs. Mathematical energy proofs are used to show that an initial boundary value problem will have a unique solution, and that the error will remain bounded for small perturbations, for a period of time. An ill-posed system can have unbounded growth of its high-frequency components, which can lead to large errors in the solution or an exponential explosion. Kreiss and Lorenz (1989) discuss well-posedness beginning with simple linear constant-coefficient systems and proceed to the nonlinear equation sets of interest to meteorology, such as (1)–(5). Browning and Kreiss (1986) provide the scaling and analysis needed to apply the theory to systems with multiple timescales, such as atmospheric prediction.

The theory for accurate and stable modeling is not only related to boundary conditions. It prescribes conditions on the degree of symmetry in the governing equations, the smoothness in the initial and boundary conditions, and the smoothness in the forcing terms. The effect of the nonhydrostatic parameter α , [which is typically set to 0.01 for the $O(100\text{-km})$ scale], is to make the equation set more symmetric (or equivalently, less skewed) for the gravity wave term. Conversely, a pure nonhydrostatic model ($\alpha = 1$) is more skewed and should have larger gravity wave vertical velocity responses to small perturbations as discussed in section 3f. It has been shown (Oliger and Sundstrom 1978) that the use of the hydrostatic, primitive equations for a limited area leads to an ill-posed boundary-value problem. A fully nonhydrostatic model can be made well posed if it is properly done; however, as commonly implemented with implicit formulations for the vertical co-

ordinate, or time splitting for the horizontal, the well posedness for larger scales is questionable (Browning and Kreiss 1994b). A quasi-nonhydrostatic model can be made well posed and is less sensitive to errors than a fully nonhydrostatic model.

c. Classification of quasi-nonhydrostatic models

The parameter, α , which is used in the vertical equation of motion, should be determined by the square of the aspect ratio of the phenomena of interest (Browning and Kreiss 1986). Taking the scale height of the atmosphere to be 10 km, if one wishes to accurately compute horizontal waves of wavelength 100 km, the associated aspect ratio would be

$$\alpha = [(10 \text{ km})/(100 \text{ km})]^2 = 10^{-2}.$$

Thus, to obtain the best accuracy for mesobeta (as defined by Orlanski 1975) motions, one would use a model with a vertical equation of motion of the form

$$dw/dt = 0.01 \left(\frac{1}{\rho_0} \frac{dp}{dz} - g\theta \right).$$

To simplify the discussion, we have classified the QNH model by the magnitude of the negative exponent, henceforth referred to as the quasi-nonhydrostatic “class.” Thus, the model discussed above with $\alpha = 10^{-2}$ would be a QNH2 class, and a mesoalpha-scale model with a square aspect ratio of 10^{-4} would be a QNH4.

Figure 1 gives examples of quasi-nonhydrostatic models classes, and typical atmospheric phenomena for which they would be appropriate. Figure 1 shows that a fully nonhydrostatic model should be used for phenomena such as individual cumulonimbus towers or steep mountain-induced gravity waves, while the mesobeta phenomena such as fronts, orographic precipitation, and squall lines can be predicted accurately using a QNH2 class model. An interesting aspect of the work of Browning and Kreiss (1986) is that even for large scales, a QNH6 model should be more accurate and have more well-behaved vertical velocity fields (and thus precipitation fields) than a hydrostatic model. This is a very important result that could be valuable in lower-resolution models, such as those used for long-term climate simulations.

d. Bounded derivative initialization

Since the QNH model is a hyperbolic system with multiple timescales, a limited-area model can be initialized using the bounded derivative approach. Browning et al. (1980) discuss a systematic procedure for determining the equations to achieve the desired accuracy in the bounded derivative approach.

An important aspect of use of bounded derivative initialization, which may be valuable in mesoscale


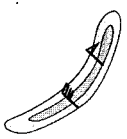

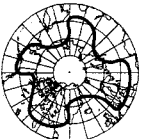
					
Examples of phenomena best represented	Cumulonimbus	Fronts, terrain, forced precipitation, squall lines, cloud clusters, hurricane band	Mid-latitude short wave	Mid-latitude long wave	
Scale (After Orlandi, 1975)	Meso-gamma	Meso-beta	Meso-alpha	Macro	
Horizontal Length Scale, L	$10^{\frac{N+2}{2}}$ km	10 km	100 km	1000 km	10,000 km
Aspect Ratio H/L	$10^{\frac{-N}{2}}$	1	$\frac{1}{10}$	$\frac{1}{100}$	$\frac{1}{1000}$
Vertical Acceleration Constant	10^{-N}	$10^0 = 1$	10^{-2}	10^{-4}	10^{-6}
Model Class	QNH _n	"Non-hydrostatic" QNH ₀	QNH ₂	QNH ₄	QNH ₆

FIG. 1. Classification of QNH models. They are classified by the negative of the exponent of the quasi-nonhydrostatic parameter. This is typically chosen as the square of the aspect ratio of the smallest weather phenomenon of interest. For example, a squall line with a horizontal length scale of 100 km and a vertical length scale of 10 km would have an aspect ratio of 1/10 and thus would require a QNH₂ model. The phenomena associated with each aspect ratio are shown schematically in the top row.

weather prediction, concerns forcing such as heating (or friction). The technique allows for initialization with a heating function explicitly accounted. Heating shows up on the right side of Eq. (5) and if heating is known as a function of space, it can be incorporated into the initial balance. Because heating can often be estimated from independent data sources, such as radar (to estimate latent heating), satellite (allowing estimates of radiative heating as well as latent heating), and surface precipitation rates, it can be used as a purely diagnostic input into the bounded derivative initialization. In other words, if heating is accurately known as a function of space (and time) it can be used with the basic equation sets (1)–(5). A more complex situation, not tested or discussed here, is to attempt a bounded derivative initialization with a full set of bulk moisture equations in addition to the dynamic equations.

The implementation of the bounded derivative technique for QNH is detailed in Lee and MacDonald (2000). Based on the second-order bounded derivative initialization, two dynamic constraints are derived to suppress the fast acoustic waves corresponding to the two largest eigenvalues in the system. These two constraint equations lead to two elliptic equations formulated on the terrain following coordinate to account for the complex terrain. One of the main advantages in using the bounded derivative initialization is to obtain balanced lateral boundary data for a limited-area prediction model through the formulation of well-posed boundary conditions for the elliptic equations.

e. Well-posed boundaries

In the initial boundary value problem considered by Olinger and Sundstrom (1978) it is shown that no well-posed pointwise boundary conditions can be assigned in a model that has the hydrostatic assumption. Intuitively, the pressure can be assigned according to the weight of the air above (i.e., hydrostatic), or a value that allows high-speed waves to propagate in and out of the open boundary of the domain, but not both. The quasi-nonhydrostatic models, as well as pure nonhydrostatic models, can have well-posed boundaries, provided certain requirements are met.

Almost all limited-area mesoscale weather models must deal with open boundaries, and ideally, as stated by Olinger and Sundstrom (1978), "(open) boundaries should determine the interior flow as though, in fact, the boundaries were not there at all." Their approach is to use the methods developed by Kreiss (1970) to form boundary conditions, which can be shown by energy inequalities to limit error growth rates (in response to perturbations in initial and boundary conditions, and forcing) as the theory requires. The applicability of such boundary conditions to models that are not well posed in other respects is thus questionable. For a well-posed model such as QNH, well-posed boundaries allow (but do not guarantee) all the waves—Rossby, gravity, and acoustic—smooth transmission into and out of a limited domain. Note that even with well-posed boundaries, it is possible for differences between the models used in

an inner and outer domains to generate high gradients in the dependant variables, or other similar problems at the boundary. It is noted in passing that such a model taken collectively (i.e., the inner plus the outer domain) would not meet Kreiss's (1980) definition of smoothness and thus would not be well posed. A typical example of such problems occurs when the physics packages, such as moisture or radiation, result in forcing that generates substantial difference in evolution of the inner and outer domains. Stated in the positive, the theory developed by Browning and Kreiss (1986) allows the implementation of an open boundary "as if it was not there at all" provided the model and the boundary are well posed, and provided that the inner and outer models are similar in their solutions.

The concepts of Olinger and Sundstrom (1978) for the open boundary problem are used for quasi-nonhydrostatic models. The procedure for assigning boundary values that are well posed can be illustrated in one dimension for horizontally propagating waves. Taking the western boundary as an example, the characteristics of the waves of the outer coarse-mesh model enter the domain from the west, and the inner fine-mesh model has waves that are exiting from the east:

$(u_c + sp_c)$ Coarse mesh (incoming) characteristic

$(u_f - sp_f)$ Fine mesh (outgoing) characteristic,

where s is defined as

$$s = (\rho_0 \gamma P_0)^{1/2}.$$

These equations must be satisfied for both incoming and outgoing waves. We define a value of u^* and p^* at the boundary that can satisfy both:

$$u^* + sp^* = u_c + sp_c \quad (6)$$

$$u^* - sp^* = u_f - sp_f, \quad (7)$$

where the subscript c denotes the value on the coarse mesh, and the subscript f denotes the value on the fine mesh.

These two equations in two unknowns can be solved for u^* and p^* . The other dependent variables, v , w , and θ , are determined from the coarse mesh or the fine mesh depending on the west wind direction determined from the fine-mesh prediction. If u_f is greater than 0, the values of v , w , and θ , are taken from the coarse (outer) mesh, and if u_f is less than 0, they are extrapolated from the fine (inner) mesh.

Typically we use a linear second-order extrapolation from the interior to the boundary for u_f and p_f

$$u_f(I = 0) = 1.5u_f(I = 1) - 0.5u_f(I = 2)$$

$$p_f(I = 0) = 1.5p_f(I = 1) - 0.5p_f(I = 2).$$

These equations need to be modified for staggered and other types of grids.

Solving for the well-posed values gives

$$u^* = \frac{1}{2}[u_c + u_f + s(p_c - p_f)]$$

$$p^* = \frac{1}{2s}(u_c + u_f) + \frac{1}{2}(p_c - p_f).$$

Generalization of this approach to other lateral boundaries and the top boundary is straightforward.

In order to illustrate the results of use of a well-posed boundary, we ran a simple experiment. The fully non-hydrostatic version of the QNH model was initialized at rest and forced with a 1-J heat impulse during the first minute of integration. The impulse was Gaussian in time and space, with a 30-s rise and fall time of the heating, and an e -fold radius of 40 km in the horizontal, and 1 km in the vertical. The impulse was located at 5500 m in the midtroposphere. The result of the experiment is shown in Fig. 2. Figure 2a is the vertical velocity at the location of the impulse center, with a rigid lid used for the upper boundary condition. Figure 2b is the vertical velocity at the same location, but for a run in which the well-posed upper boundary condition was used. In this graph of the first hour there are two waves evident. The fast wave is an acoustic wave, and it is clear that the well-posed boundary greatly decreased the reflection of the acoustic wave back into the domain. The second wave is the gravity wave, which is similar in both integrations. Our experience with well-posed boundaries show that they are particularly helpful near the boundaries but also significantly decrease the spurious buildup of reflected acoustic and gravity wave energy throughout the domain of a limited-area model.

f. Smoothness

Kreiss's (1980) theory for hyperbolic systems with multiple timescales includes the concept of mathematical "smoothness" for variables in both time and space. In order to separate the meteorologically significant "slow" motions from the fast waves, which do not require deterministic prediction, smoothness is required in the initial fields and forcing. In practice, this means that the space derivatives of first and higher order must be of order one in a scaled version of the system, and they must be smooth up to the boundary. In other words, a discontinuity between the interior and the boundary will violate the smoothness assumption required in the energy proof that constrains the time variation. It is shown in Browning and Kreiss (1986) that the solution of an equation set like (1)–(5) can be made smooth near the boundaries by setting the constant α equal to the square of the aspect ration of the meteorological phenomena being modeled:

$$\alpha \sim (\text{vertical phenomena scale} \\ \div \text{horizontal phenomena scale})^2.$$

There is another important ramification of the concept of smoothness. Physical phenomena such as turbulence,

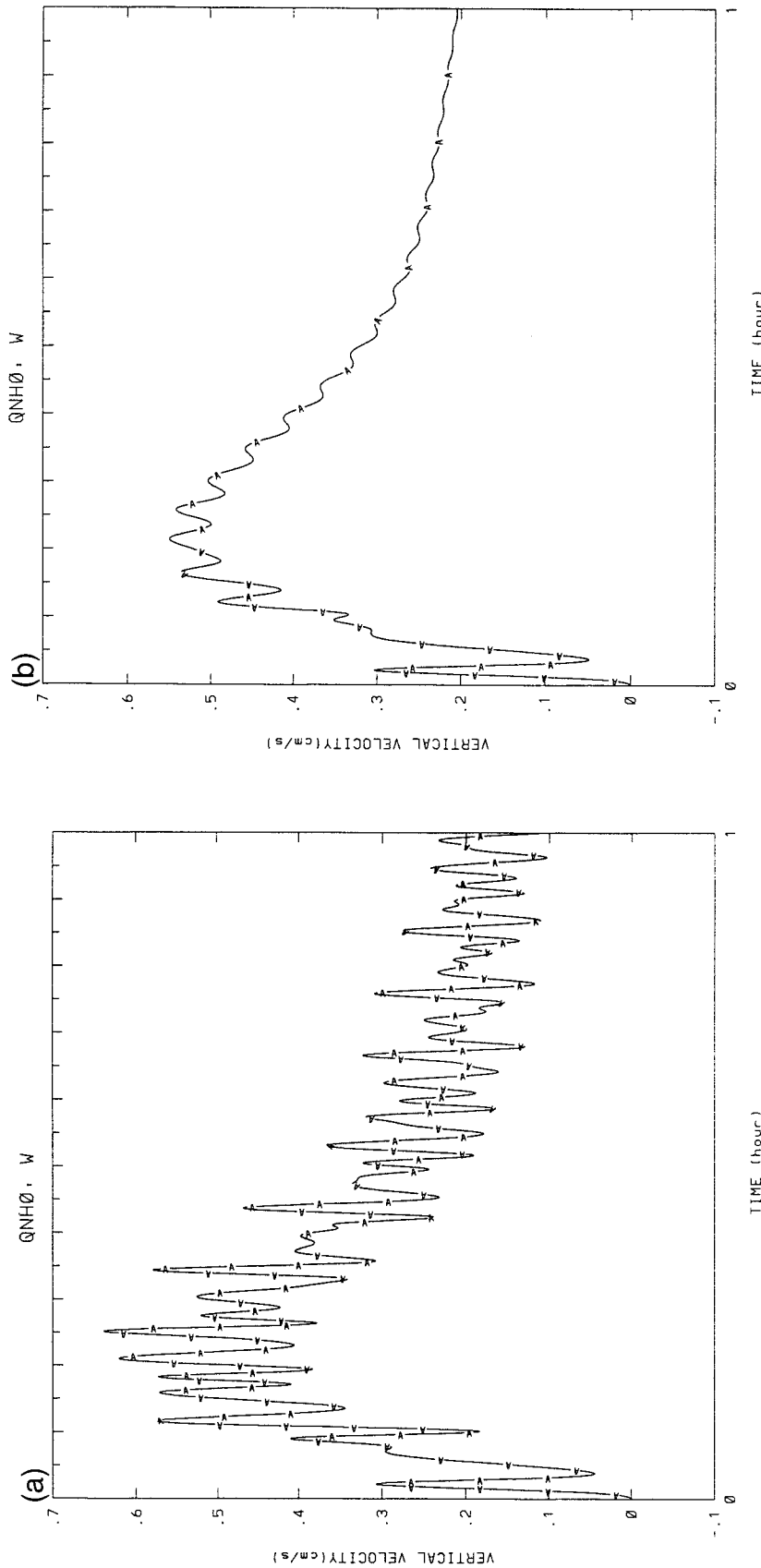


FIG. 2. An illustration of the effect of a well-posed upper boundary on a fully nonhydrostatic version of the QNH model. A heating impulse of 1 J was applied to a 3D Gaussian domain for 1 min right after the model integration was initiated. The domain had e -fold radius of 40 km in the horizontal, 1 km in the vertical, and was located at 5.5 km in the midtroposphere. The impulse generated a gravity wave that peaked and decayed in the first hour, as well as acoustic waves. (a) With a rigid lid as an upper boundary, the acoustic waves that are high frequency and have an amplitude of $0.1\text{--}0.2\text{ cm s}^{-1}$ are clearly excited. (b) With a well-posed boundary, the acoustic waves show weakly after the initial impulse but soon die out.

latent heating, and radiation enter the dynamics through forcing terms in sets (1)–(5). If these are not mathematically smooth, they can generate perturbations and fast waves that degrade the meteorologically significant part of the solution. This means that physics package forcing terms, such as heating that will enter on the right side of Eq. (5), must be smooth. This issue is discussed extensively in Browning and Kreiss (1994a). In practice, smoothness in a quasi-nonhydrostatic model can be enforced after the calculation, but before the forcing is injected into the dynamics equations. Browning and Kreiss (1994a) refer to small-scale perturbations in forcing (e.g., heating at a single grid point), which appear in full-physics model integrations as “rough forcing.” They show that high spatial gradients that appear as a result of rough forcing can generate high-frequency waves, which at best degrade the solution and which may lead to instability and diverging solutions. The use of large explicit or implicit diffusion damping can also degrade the solution, affecting the slow-mode meteorological waves of interest in an effort to keep the high-frequency waves in check.

g. Explicit calculation

An interesting aspect of the use of the quasi-nonhydrostatic parameter is that it allows a completely explicit formulation of a model. Browning and Kreiss (1986) referred to two types of well-posed models; one they referred to as the approximate system, which is the type of model discussed in this paper. The second, called the “reduced system,” is a system in which an elliptic equation must be solved to relate pressure and velocity in the forward integration of the model. The trade-off of a purely explicit system, in which time steps must be quite short to meet CFL criteria, and a system that requires solution of elliptic equations is complex. It is possible that the savings in making fewer time steps with implicit techniques can overcome the increased computing requirements, which solution of elliptic equations creates. However, in addition to purely numerical considerations, it is important to consider the effect that long time steps have on gravity wave solutions, which in the mesoscale can have timescales of minutes. Part of our reason for the use of the approximate or quasi-nonhydrostatic formulation is that it results in a simplicity of development in the resulting computer code. Explicit codes are also quite amenable to advanced computer capabilities; the QNH model is parallelized in the horizontal and vectorized in the vertical direction. A major purpose in the development of the QNH model was to determine the advantages and disadvantages that a purely explicit model would have.

Quasi-nonhydrostatic models can be explicit in their vertical calculations because one effect of the constant α is to slow down the vertical acoustic waves. The modeler can choose the constant so that the time needed for an acoustic wave to cross a grid length in the vertical

is the same as the time needed to cross a horizontal grid length. The vertical acoustic wave has a phase velocity, c_v , given by

$$c_v = \sqrt{\alpha} \sqrt{\frac{\gamma P_0}{\rho_0}}.$$

Similarly, the horizontal acoustic velocity is given by

$$c_h = \sqrt{\frac{\gamma P_0}{\rho_0}}.$$

Since $\sqrt{\alpha} = \Delta z / \Delta x$,

$$c_v = (\Delta z / \Delta x) c_h.$$

Thus, it is most efficient to choose α and the vertical and horizontal grid mesh distances such that the CFL criteria in the horizontal and vertical directions are identical.

Most nonhydrostatic models use an implicit formulation for the vertical coordinate calculations, which obviates the difficulties associated with vertical CFL requirements. Browning and Kreiss (1994b) have indicated that the semi-implicit vertical formulation reduces in a mathematical sense to a primitive equation formulation, and therefore such models are ill posed.

3. Wave analysis

The nature of a quasi-nonhydrostatic model can be best understood by analyzing its effects on various atmospheric waves. For purposes of discussion, we classify waves as “free” or “forced.” Free waves are the internal waves that are solutions of the eigensystem, that is, Rossby, gravity, and acoustic waves. The linear system analysis is presented in section 3a, followed by a discussion of the effect of the quasi-nonhydrostatic parameter on the free waves; Rossby waves in section 3b; and gravity waves in section 3c. Then the effect of the quasi-nonhydrostatic parameter on forced waves is discussed; heat-forced circulations in section 3b and terrain-forced gravity waves in section 3e. Finally, the response of the quasi-nonhydrostatic system to unbalanced perturbations in the initial state and heating impulses is presented in section 3f. It is shown that the quasi-nonhydrostatic model does not affect the Rossby and heat-forced circulations. Conversely, gravity waves are selectively modified, with larger scales unaffected, and small-horizontal, large vertical-scale waves decreased in both frequency and amplitude. Vertical acoustic waves are slowed down, which slows down the hydrostatic adjustment process.

a. Linear analysis

In order to illustrate the role of the free waves in a quasi-nonhydrostatic model, we analyze a linearized, somewhat simplified version of Eqs. (1)–(5). This analysis is detailed in appendix A and summarized here to

support the associated discussion. We assume the mean flow is zero and drop smaller terms to get

$$\frac{\partial u}{\partial t} = -\frac{1}{\rho_0} \frac{\partial p}{\partial x} + fv \quad (8)$$

$$\frac{\partial v}{\partial t} = -\frac{1}{\rho_0} \frac{\partial p}{\partial y} - fu \quad (9)$$

$$\frac{\partial w}{\partial t} = \alpha \left(-\frac{1}{\rho_0} \frac{\partial p}{\partial z} + g\theta \right) \quad (10)$$

$$\frac{\partial p}{\partial t} = -\gamma P_0 \left(\frac{\partial u}{\partial x} + \frac{\partial v}{\partial y} + \frac{\partial w}{\partial z} \right) \quad (11)$$

$$\frac{\partial \theta}{\partial t} = -\tilde{\theta} w. \quad (12)$$

To simplify the discussion of pure gravity waves, we will drop the Coriolis parameter in the subsequent analysis. To a good approximation, the eigenvalues for the system are

$$\omega_1 = 0 \quad \omega_2 = -\omega_4 \approx \left[\frac{g\tilde{\theta}(k^2 + l^2)}{\alpha^{-1}(k^2 + l^2) + m^2} \right]^{1/2}$$

$$\omega_3 = -\omega_5 \approx C_s^2 [(k^2 + l^2) + \alpha m^2]^{1/2},$$

where $C_s = (\gamma P_0 / \rho_0)^{1/2}$, the speed of sound.

These five eigenvalues represent frequencies associated with acoustic, gravity, and Rossby waves. When solved for the eigenvectors we get the Rossby wave eigenvector as

$$(\hat{u}, \hat{v}, \hat{w}, \hat{p}, \hat{\theta}) = (l, -k, 0, 0, 0)$$

and for other nonzero eigenvalues, ω_i , the eigenvectors are

$$\begin{bmatrix} \hat{u} \\ \hat{v} \\ \hat{w} \\ \hat{p} \\ \hat{\theta} \end{bmatrix} = \begin{bmatrix} -\omega_j^{-1} i \rho_0^{-1} k \hat{p} \\ -\omega_j^{-1} i \rho_0^{-1} l \hat{p} \\ -\tilde{\theta}^{-1} \omega_j \\ \hat{p}_j \\ 1 \end{bmatrix},$$

where

$$\hat{p}_j = (i \rho_0^{-1} m)^{-1} (g + \tilde{\theta}^{-1} \alpha^{-1} \omega_j^2).$$

This system allows analysis of the effect of the quasi-nonhydrostatic parameter, α , on the three types of waves. It can be seen that α affects the frequency of sound waves with vertical structure, but not, for example, horizontal sound waves such as the Lamb wave. As discussed in section 2g, the speed of propagation of sound waves in the horizontal is unchanged, but their propagation in the vertical is slowed down.

b. Rossby waves

The linear analysis above demonstrates that the parameter α does not affect the frequency or amplitude of

the Rossby waves. We would like to extend the analysis to a simple nonlinear steady-state system with a secondary circulation. This can be done by deriving a vorticity equation from Eqs. (1) and (2), and assuming incompressibility to obtain

$$u \frac{\partial \zeta}{\partial x} + f \left(\frac{\partial u}{\partial x} + \frac{\partial v}{\partial y} \right) = 0 \quad u \frac{\partial \theta}{\partial x} + w \tilde{\theta} = \frac{h}{C_p T}$$

$$\frac{\partial u}{\partial x} + \frac{\partial v}{\partial y} + \frac{\partial w}{\partial z} = 0,$$

where h is heating, and ζ is the relative vorticity.

For the case in which there is no heating with the zonal mean wind independent of space and time, the system can be combined into a single equation:

$$u \frac{\partial \zeta}{\partial x} = \frac{fu}{\tilde{\theta}} \frac{\partial^2 \theta}{\partial x \partial z}.$$

We can determine a horizontal length scale for this system by solving for it in terms of the other variables:

$$L \sim \frac{UH\tilde{\theta}}{f\theta} \sim 10^6 \text{ m},$$

where

$$U \sim 10 \text{ m s}^{-1}, \quad H \sim 10^4 \text{ m}, \quad \theta \sim 10^{-2},$$

$$f \sim 10^{-4} \text{ s}^{-1}.$$

Thus, the simple nonlinear system with a steady-state ageostrophic component scales to the 1000-km scale. A more complete analysis of this type is presented in Browning and Kreiss (1986). The main point of the discussion is to show that the quasi-nonhydrostatic system should accommodate Rossby waves with ageostrophic secondary circulations and still have appropriate horizontal length scales. A similar analysis with heating included yields a horizontal length scale of 100 km, again unaffected by the quasi-nonhydrostatic parameter.

c. Gravity wave analysis

From the analysis in section 3a, dispersion equation for gravity waves is given by

$$\omega_g = \left[\frac{N^2(k^2 + l^2)}{\alpha^{-1}(k^2 + l^2) + m^2} \right]^{1/2},$$

where $N^2 = g\tilde{\theta}$ is the buoyancy or Brunt–Väisälä frequency, which are synonymous. The quasi-nonhydrostatic parameter shows up in the frequency of the gravity modes for all of the variables, and in the amplitude of the vertical velocity. To examine this effect, we define a frequency reduction

$$\text{Frequency reduction} = \frac{\omega(\alpha = 1) - \omega(\alpha = 10^{\text{NE}})}{\omega(\alpha = 1)},$$

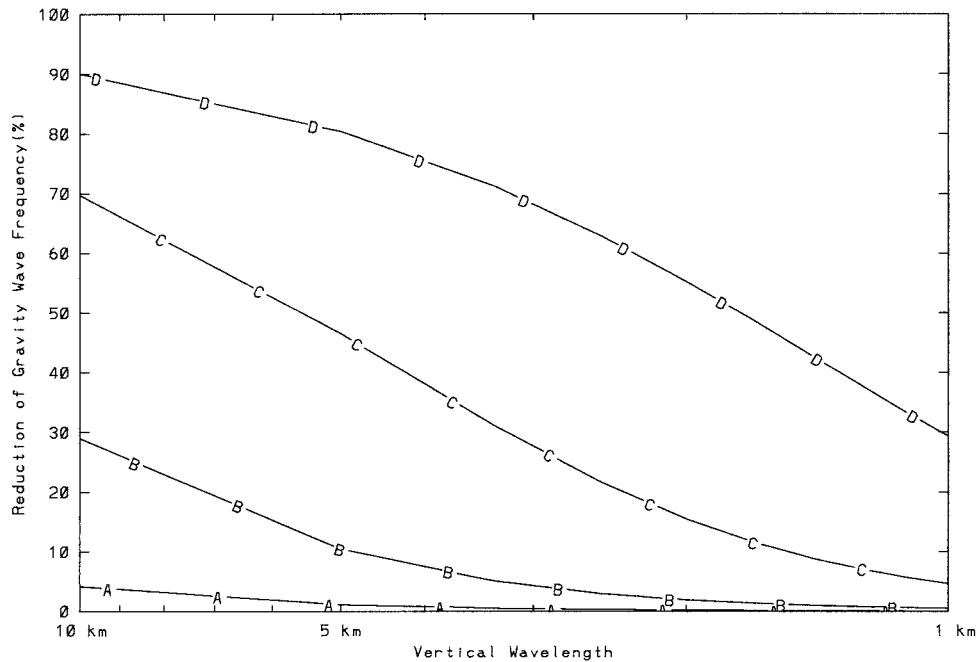


FIG. 3. Reduction of the gravity wave frequency of an $O(100\text{-km})$ wave as a function of the vertical wavelength. Line A–A–A would be for $\alpha = 10^{-1}$, line B–B–B for $\alpha = 10^{-2}$, line C–C–C for $\alpha = 10^{-3}$, and line D–D–D for $\alpha = 10^{-4}$. The frequency of the gravity wave is quite accurate for all vertical wavelengths for the QNH1 version of the model (line A–A–A). The QNH2 model (line B–B–B) is quite accurate for vertical gravity waves of wavelength less than a few kilometers. It has about a 10% frequency reduction for gravity waves of vertical wavelength 5 km and has nearly a 30% frequency reduction for wavelengths of the full scale height of the atmosphere (10 km). The QNH3 and QNH4 models substantially decrease the frequencies of gravity waves for all vertical wavelengths.

where NE = negative of the exponent of the quasi-nonhydrostatic constant α .

The frequency reduction due to the quasi-nonhydrostatic parameter is a function of vertical wavelength. Figure 3 shows the frequency reduction of an $O(100\text{-km})$ horizontal gravity wave as a function of height for different α 's. It is clear that when $\alpha = 10^{-2}$, the reductions are quite small for vertical wavelengths on the order of 1 km, while they become substantial for vertical wavelengths approaching the scale height of the atmosphere. Free gravity waves, which will be discussed in the remainder of this section, typically have small vertical wavelengths, and associated small-frequency reduction. Terrain-forced gravity waves, discussed in section 3e, have larger vertical wavelengths and larger frequency reduction.

In order to determine the frequency reduction of free gravity waves as a function of horizontal wavelength, we must have an associated vertical wavelength. Gill (1982) discusses and approximates the aspect ratio and vertical wavelengths of atmospheric waves. Using Gill's scaling (e.g., his Table 2.1), the frequency reduction can be calculated for various quasi-nonhydrostatic constants. Figure 4 shows the frequency reduction of gravity waves for QNH1 ($\alpha = 10^{-1}$), QNH2 ($\alpha = 10^{-2}$), QNH3 ($\alpha = 10^{-3}$), and QNH4 ($\alpha = 10^{-4}$) models. There are substantial frequency reductions throughout the meso-

beta domain for the QNH4 model, as expected. The QNH3 model has substantial reduction of frequency for scales below 100 km. The QNH2 model, designed for the mesobeta scale, has only about 1% reduction for the 100-km scale (as expected by the theory, Browning and Kreiss 1986), with frequency reduction of less than 20% for the smallest mesobeta-scale waves of length 20 km. The QNH1 model is very accurate down to grid mesh sizes of 2.5 km.

The effect of α in causing a frequency reduction of the gravity waves is clearly shown in the above discussion of a linear system. However, the importance and role of gravity waves in the middle wavelengths of the mesoscale is complex. Browning and Kreiss (1997) show that the energy in gravity waves at these scales is quite small. They point out that it is difficult to distinguish phenomena due to forcing from heating from that due to free gravity waves and argue that some observational studies have confused gravity and heat-forced waves.

d. Heat-forced circulations

It is characteristic of the mesoscale that forcing such as that due to heating and frictional effects is ubiquitous and important. In real prediction models, circulations can be created by sustained forcing, such as latent heat-

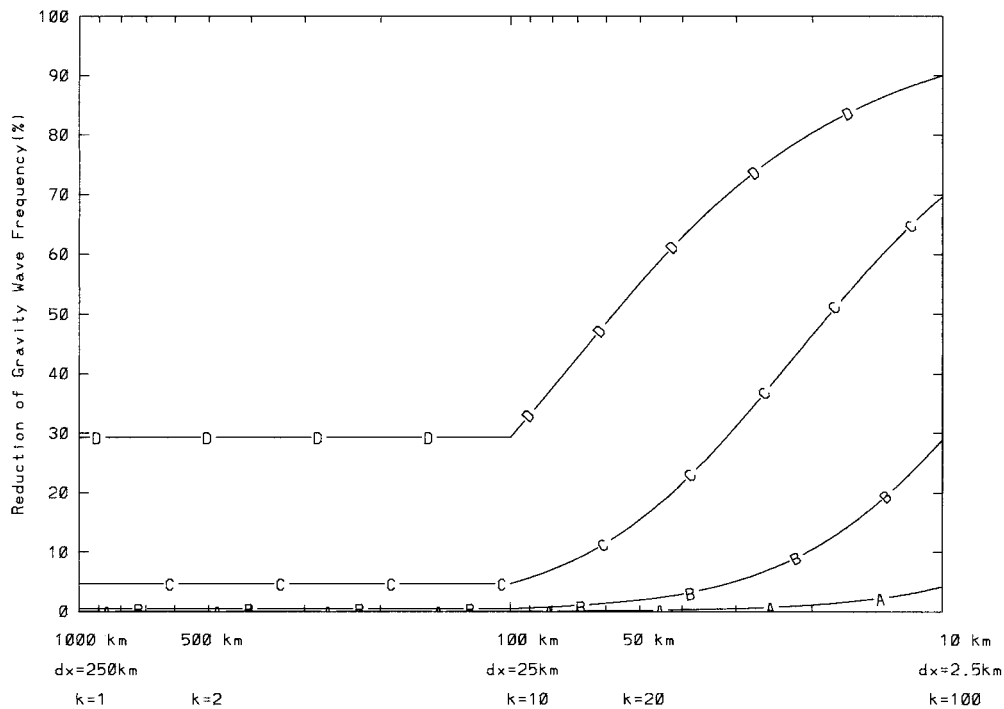


FIG. 4. Reduction of frequency for free gravity waves with vertical wavelengths as scaled by Gill (1982). Line A–A–A is for the QNH1 model, with $\alpha = 10^{-1}$, line B–B–B for the QNH2 model, line C–C–C for the QNH3 model, and line D–D–D for the QNH4 model. The QNH1 is accurate for free gravity waves at all wavelengths. The QNH2, with $\alpha = 10^{-2}$ is quite accurate until horizontal wavelengths become less than 50 km. The QNH3 model shows a large decrease in free gravity wave frequency for waves less than 50-km wavelength. The QNH4 decreases free gravity wave frequencies for all wavelengths.

ing associated with a mesobeta-scale precipitation. In addition, as higher and higher resolutions are used, there are often strong impulses of heating due to convective instabilities and other small-scale phenomena. In this section, we examine the adjustment of a quasi-nonhydrostatic model to sustained forcing and in section 3f, the responses to impulses in forcing as well as perturbations in initial conditions are discussed.

From a modeler's viewpoint, the salient characteristic of a quasi-nonhydrostatic model is its smoothness and stability. The fact that the model should be more stable can be shown mathematically (e.g., Browning and Kreiss 1985), but what is really happening? It will be argued that vertical velocity gravity-mode response to deep perturbations, either in initial conditions or forcing, are decreased in frequency and smaller in amplitude, and that this is the reason for the stability of the model for appropriate length scales. This change in frequency and amplitude of the small-scale, deep gravity waves could be regarded as an error if deterministic prediction of individual gravity waves was the goal, or if the effect is to change the balanced state of the model away from that appropriate to the Rossby waves, and forcing due to terrain effects and heating. We argue here that the quasi-nonhydrostatic parameter can be chosen such that the model properly predicts the Rossby and forced cir-

ulation for any length scale, while the high-frequency gravity modes are suppressed.

It is important to make a distinction between stability, error growth rates, and the accuracy of a model weather forecast. As has been discussed, a quasi-nonhydrostatic model should be more stable and have smaller error growth rates than either hydrostatic models or pure nonhydrostatic models. This does not always guarantee that the quasi-nonhydrostatic model will make a more accurate weather forecast. It could be made more accurate if its inherent stability allowed the model integration to occur with less dissipation, but that effect could be counteracted by its artificially reduced rate of hydrostatic adjustment.

We will discuss vertical velocity, which is very important because it is the dynamic field that is most closely related to cloud and precipitation. The role of gravity waves in slowly varying mesoscale motions has recently been addressed by Browning and Kreiss (1997). They derive a version of the dynamic equations that does not admit gravity waves to show that the dominant component of some slowly varying mesoscale motions is not due to gravity waves, but rather is forced, typically by heating. They show that gravity wave vertical velocities are typically an order of magnitude smaller than the heat-forced vertical velocity fields.

In simple terms, gravity waves are related to the buoyancy term in the vertical velocity equation, and the stability term in the thermodynamic equation. A simplified version of these two equations, with the addition of a heating term, is

$$\frac{dw}{dt} = -\frac{\alpha}{\rho_0} \frac{\partial p}{\partial z} + \overbrace{\alpha g \theta}^{\text{Buoyancy term}}, \quad \frac{d\theta}{dt} = \overbrace{-\tilde{\theta} w}^{\text{Stability term}} + \overbrace{\frac{h}{C_p T}}^{\text{Heating term}},$$

where h is heating in W kg^{-1} . It is crucial to distinguish between the gravity mode (buoyancy and stability terms) and the balance that is possible between the heating term and the stability term in the thermodynamic equation. Ignoring vertical pressure gradient and heating, the cross-diagonal buoyancy and stability terms combine to give a wave equation with the buoyancy frequency clearly in evidence:

$$\frac{d^2 w}{dt^2} = -N^2 w.$$

Typically, the frequency of gravity waves is $N = 10^{-2} \text{ s}^{-1}$. The complete analysis, given in appendix A, shows that this frequency is modified by the vertical and horizontal wavelengths of the gravity wave. As pointed out in Browning and Kreiss (1997), a slow mode circulation can develop due to latent heat forcing, with a balance being established between the heating term and the compensating cooling due to upward motion:

$$\tilde{\theta} w = \frac{h}{C_p T}. \quad (13)$$

While this is not a wave in the same sense as a gravity wave, confusion between the two is common. Scale analysis can be used to illustrate the balance between the two terms. For deep tropospheric precipitation at a rate of 5 mm h^{-1} (1 W kg^{-1}) over a 100-km area, scaling shows that

$$u \frac{\partial \theta}{\partial x} \sim 3 \times 10^{-7}; \quad \tilde{\theta} w \sim 3 \times 10^{-6};$$

$$\frac{h}{C_p T} \sim 3 \times 10^{-6}.$$

Note that θ is perturbation potential temperature, as defined in Section 2b. The heating and vertical velocity terms are in balance, approximately one order of magnitude larger than the potential temperature advection term. It has been shown (Browning and Kreiss 1997) that the response of a well-posed model to smooth forcing, such as that resulting from precipitation-forced latent heating, will be properly accommodated by the balance between the stability and heating terms in the thermodynamic equation.

We did an experiment with the full QNH model to illustrate its adjustment to steady heating. A Gaussian

region of heating was applied for both a fully nonhydrostatic version of the model (QNH0) and for the model that is appropriate for mesobeta scale use (QNH2). The heating had an e -fold radius of 100 km in the horizontal, and 4 km in the vertical, with an amplitude of 1 J kg^{-1} . It was centered at 5500 m in the midtroposphere and has an equilibrium vertical velocity of 33 cm s^{-1} . Figure 5a shows that the fully nonhydrostatic version of the model adjusts to the proper vertical velocity in a little more than 1 h. The vertical velocity is graphed through 6 h at the center point of the heating. Figure 5b shows the vertical velocity for a QNH2 run. The effect of the quasi-nonhydrostatic constant, $\alpha = 10^{-2}$, is to create a slight overshoot and adjustment in the period between 1 and 3 h. It is notable that the rise of vertical velocity during the first hour is almost identical in the two runs. It is clear that the constant α does not have a significant detrimental effect on the adjustment to forcing, as discussed above. A smaller quasi-nonhydrostatic constant would result in a slower hydrostatic adjustment.

Although it is important that the model maintain a proper balance between the heating and compensating vertical motion, it is not a necessity that the balance occur the same way in a model as in the real atmosphere. It has been argued that the adjustment to heating occurs through the action of gravity waves. Unless the purpose is to deterministically predict the individual gravity waves, the important thing for mesoscale models is that the right adjustment takes place. In fact, many cases where gravity waves have been identified as releasing convective instability are cases where a QNH2 model would have properly predicted the phenomenon, although a QNH3, with its larger suppression of gravity waves, may not have. For example, observational studies (Yang and Houze 1995) have shown gravity waves playing a role in creating the multicell structure of squall lines. A QNH1 model should properly accommodate such a process, while a QNH2 should have reasonable heating and precipitation, with lack of detail in the finescale structure of squall lines.

Orlanski (1980) discussed the difficulties of hydrostatic models for mesoscale prediction of precipitation. Starting with the full dispersion equation for gravity waves, he showed that an effect of the hydrostatic assumption is to make small-scale moist convection unstable in hydrostatic models. On this basis, it is regarded that the quasi-nonhydrostatic approach should be better for precipitation prediction than hydrostatic models. Orlanski (1980) used an expansion in terms of the aspect ratio (equivalent to the square root of the quasi-nonhydrostatic constant) to define a quasi-hydrostatic model. This is a different approach than that developed by Browning and Kreiss (1986), but as shown in the paper, has some of the advantages of the quasi-nonhydrostatic approach. Specifically, the unstable character of the mesobeta-scale moist convection is ameliorated; however, the quasi-hydrostatic approach is still ill posed and will have associated and stability problems.

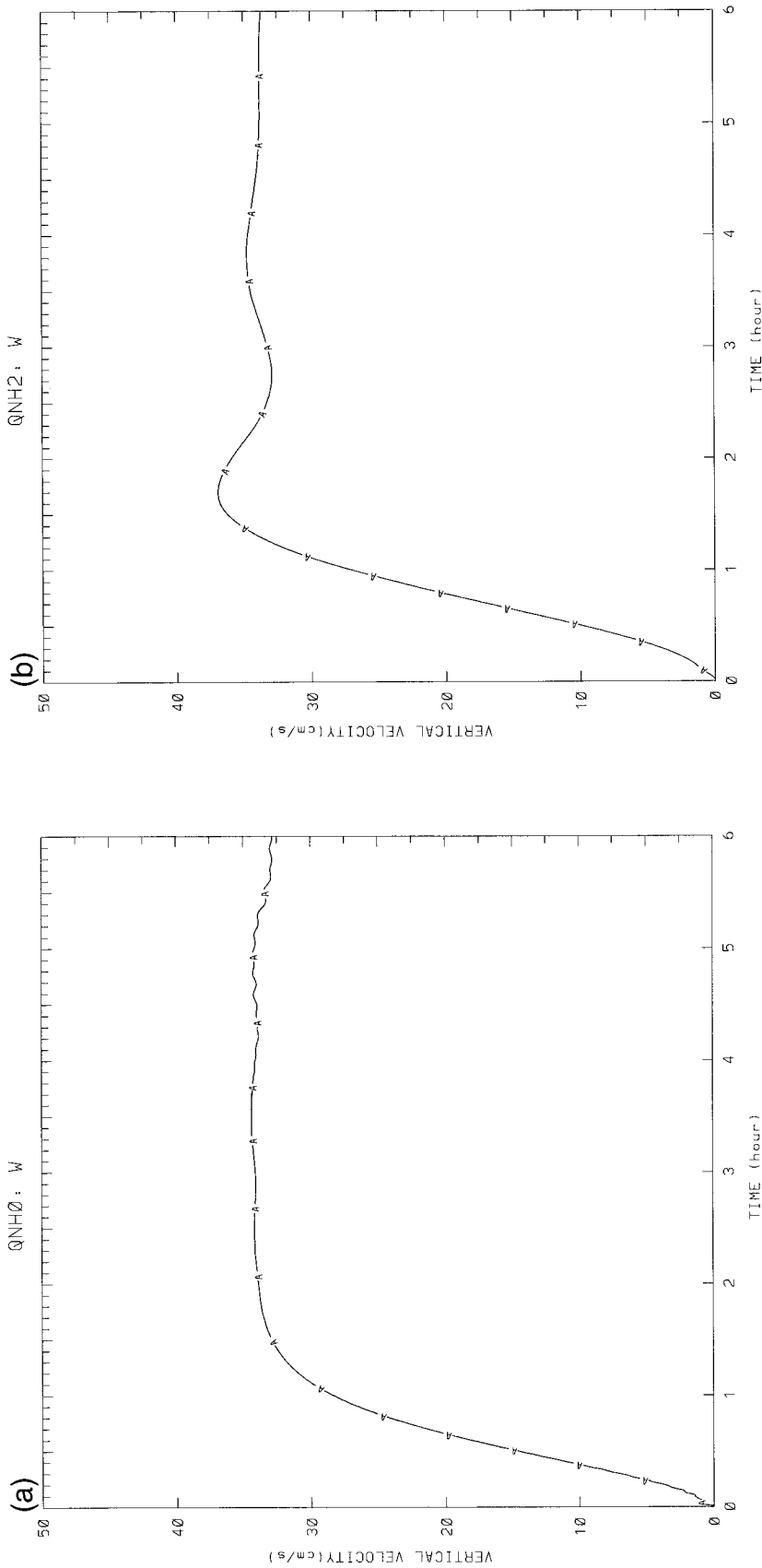


FIG. 5. Response of models to steady heating. Steady heating of 1 J kg^{-1} was applied at the 5.5-km level in the center of a $640 \text{ km} \times 640 \text{ km}$ domain. The heating was applied in a 3D Gaussian form, with horizontal e -fold radius of 100 km and vertical e -fold radius of 4 km. In (a), the response of the fully nonhydrostatic version of the QNH model (i.e., $\alpha = 1$) is shown. The vertical velocity rises over the period of an hour to a steady value of about 33 cm s^{-1} . In (b), the same graph is plotted for the QNH2 model; the vertical velocity is very similar, rising on exactly the same timescale, with a slight overshoot, and steadying out at 33 cm s^{-1} . The proper adjustment to steady heat forcing is a crucial property of quasi-nonhydrostatic models.

e. Terrain-forced gravity waves

Terrain-forced gravity waves have important effects and are quite different from free gravity waves (e.g., they typically have larger vertical wavelengths). Effects include flux of energy from the surface into the atmosphere and downslope windstorms. There is also an effect on numerical prediction when gravity modes are accommodated by model equation systems with inadequate spatial resolution, unstable amplification of errors, or other approximations in formulation; the result may be generation of fields that detract from the accuracy of prediction. Operational models are only now reaching the horizontal resolutions where terrain-forced hydrostatic, nonrotating gravity waves can be properly accommodated.

The frequency of gravity wave forcing from underlying terrain caused by uniform flow of air over it is

$$\omega = Uk,$$

where ω is the frequency, U is the horizontal velocity, and k is the horizontal wavenumber.

Setting the frequency forced by terrain equal to the frequency for the linear solution gravity wave, and solving for the vertical wavenumber, m , gives

$$m = \left(\frac{N^2}{U^2} - \frac{k^2}{\alpha} \right)^{1/2}. \quad (14)$$

This is the Scorer equation, modified by α . The effect of decreasing α is to increase the vertical wavelength. This can be seen by solving for the vertical wavelength

$$L_z = [N^2/(2\pi U)]^2 - 1/[L_x^2 \alpha]^{-1/2}, \quad (15)$$

where L_z is the vertical wavelength, and L_x is the horizontal wavelength.

Skamarock and Klemp (1994) have pointed out some difficulties of the quasi-nonhydrostatic formulation with hydrostatic terrain-forced gravity waves. It can be seen from Eq. (14) that the effect of α is to make the terrain-forced waves artificially nonhydrostatic, with a change in the critical horizontal wavelength. The critical horizontal wavelength is found by setting the argument of the square root equal to zero, and solving for the horizontal wavelength. If we assume $N^2 = 10^{-4}$, and $U = 10 \text{ m s}^{-1}$, the critical wavelength should be 6 km, but is modified to 60 km when $\alpha = 10^{-2}$ and to about 200 km when $\alpha = 10^{-3}$. The effect of the quasi-nonhydrostatic parameter on the vertical wavelength of terrain-forced waves can be seen from Eq. (15). Table 1 shows the correct vertical wavelength (i.e., with $\alpha = 1$) along with the vertical wavelength that pertains when $\alpha = 10^{-2}$. It can be seen that the wavelength is fairly accurate when $L_x = 200 \text{ km}$, becomes about 40% too large when $L_x = 100 \text{ km}$, and artificially ducts when the wavelength is 60 km or smaller. This analysis shows significant problems with terrain-forced gravity waves, in agreement with the analysis of Skamarock and Klemp (1994).

TABLE 1. Effect of the quasi-nonhydrostatic constant, α , on terrain-forced gravity waves. For terrain wavelength, the correct vertical wavelength is given when $\alpha = 1$. The effect of α is to increase vertical wavelength, resulting in ducting for waves generated by terrain forcing of 60 km or less.

Terrain wavelength (km)	Vertical wavelength (m) $\alpha = 1$	Vertical wavelength (m) $\alpha = 0.01$	Error (%)
20	6618	(Ducted)	—
40	6362	(Ducted)	—
60	6317	(Ducted)	—
80	6303	10150	61
100	6295	8076	28
120	6292	7375	17
140	6290	7031	12
160	6288	6832	9
180	6287	6704	7
200	6286	6618	5

In order to understand the effect of the quasi-nonhydrostatic parameter on terrain-forced gravity waves, we compared its solutions with the well-known Long (1953) solution for steady-state hydrostatic waves. Following the approach of Klemp and Lilly (1978) and the presentation by Pielke (1984), we used a Riemann sum to iteratively solve Pielke's Eqs. (12)–(32) that was substituted into Pielke's Eqs. (12)–(25) for solution. To obtain Long's solution, we used a bell-shaped mountain whose width was set to 100 km and height was set to 100 m. The Brunt–Väisälä frequency was set at $N = 10^{-2} \text{ s}^{-1}$ and the horizontal velocity was initialized at $U = 20 \text{ m s}^{-1}$. Both the analytic (numerically approximated) solution to Long's equation and that obtained by the QNH model are shown in Fig. 6. Figure 6a is the analytic solution for vertical velocity in cm s^{-1} (*100). Beside it, Fig. 6b is the steady-state solution obtained by running the model 12 h with the two-dimensional mountain profile. The two solutions are fairly similar, with vertical velocities differing by a maximum of 15% and a similar looking pattern with height. Close inspection reveals that while Long's solution has maxima and minima stacked very close to vertical, the QNH2 model slopes the upper-tropospheric maximum slightly to the east. The streamlines for the analytic and QNH2 model are compared in Fig. 6c. At low levels the solution is fairly accurate, but it departs significantly in the upper troposphere. Even though there are errors associated with the artificial ducting for horizontal wavelengths less than 60 km inherent in the bell-mountain shape, the overall negative effect on the solution is not excessive.

A QNH3 model should have large errors for a 100-km bell-shaped mountain because it makes the hydrostatic terrain-forced waves artificially duct throughout the mesobeta scale. This was confirmed by running the QNH3 model to obtain its steady state for the 100-km bell-shaped mountain. The analytic solution, Fig. 6a, can be compared with the QNH3 solution, Fig. 6d; its vertical velocity magnitude and pattern is incorrect with

a strong eastward slope and minimax values 50% smaller than the analytic solution. This result is in accordance with the Browning and Kreiss (1986) analysis that indicates the QNH3 should be used for mesoalpha-scale phenomena.

Despite these difficulties, we will now argue that QNH3 models may be valuable for mesobeta-scale prediction. As discussed in section 3c, the frequency reductions associated with free gravity waves are much smaller because their vertical scales are typically smaller. It is noteworthy in passing that the diffusion effects of semi-implicit formulations may make them inferior to quasi-nonhydrostatic formulations for gravity waves of small vertical wavelengths. The terrain-forced gravity wave errors in quasi-nonhydrostatic models can be limited by doing a Fourier analysis on the terrain and dropping the waves of smaller wavelength that will generate terrain-forced gravity wave errors. This approach will not generate deterministic prediction of small scale $O(100\text{-km})$ mountain waves, but it will also not detract from the accuracy by imposing an incorrect gravity mode solution on the Rossby and heat-forced circulations. In MacDonald et al. (2000), a QNH3 model with small-scale terrain filtered out was used to predict a winter storm. The resulting forecast showed that this can give reasonable results for cloud and precipitation with scales below 100 km.

A model that accurately accommodates mesobeta-scale weather must have very high resolution in the vertical $O(200\text{ m})$ and must have high-resolution terrain, with features on the order of 20 km. The best approach, for both quasi-nonhydrostatic models and nonhydrostatic models is to nest a higher-resolution domain over areas where very accurate mountain wave prediction is needed. As shown in MacDonald et al. (2000), the limiting case of a fully nonhydrostatic model (QNH0) duplicates Smith's (1980) linear three-dimensional solution for terrain-forced gravity waves.

f. Gravity mode response to perturbations

We now address an important difference between quasi-nonhydrostatic models and fully nonhydrostatic models. The two differ in their gravity wave response to perturbations in initial temperature fields and to forcing. In appendix B, the linearized quasi-nonhydrostatic equation system is analyzed for its response to a perturbation, $\delta\theta$, in the initial potential temperature field. By getting a particular solution for this simple situation, it is found that the model's gravity wave frequency shows up in both the amplitude and frequency of the gravity mode of the vertical velocity response:

$$\hat{w}(t) = \delta\theta\tilde{\theta}^{-1}\omega_g \cos(|\omega_g|t). \quad (16)$$

An analogous result can be shown to hold in physical space. The elegant and simple equation explains much about the effect of α . It does not damp the gravity waves (where damping can be thought of as a real

component of the eigenvalue), but rather, makes the response of the model to initial perturbations less in both frequency and amplitude than it would be for a purely nonhydrostatic model. As shown below, a similar result pertains for heat perturbations during the model integration.

The difference in the amplitude as well as the frequency of a gravity wave can be determined by comparing the eigenvalues of the vertical velocity solution with $\alpha = 1$ (i.e., fully nonhydrostatic), and α equal to other values (i.e., quasi-nonhydrostatic). In this analysis we use the two-dimensional dispersion equation for simplicity:

$$\omega_g = \pm \left(\frac{k^2 N^2 + m^2 f^2}{\frac{k^2}{\alpha} + m^2} \right)^{1/2}.$$

It is clear that the presence of α reduces the amplitude and frequency of the gravity wave. The physics packages in most models, including QNH, calculate heating due to moisture phase change, radiation, and turbulence in a column. Thus, perturbations often show vertical coherence. We are interested in the response to a full column perturbation in temperature or heat forcing. The two can be compared by calculating the amplitude and frequency reduction due to α as

vertical velocity perturbation response reduction

$$= \frac{\omega_g(\alpha = 1) - \omega_g(\alpha)}{\omega_g(\alpha = 1)}.$$

The reductions of amplitudes and frequencies of gravity waves as a function of horizontal wavelength are shown in Fig. 7. It can be seen that all of the QNH models reduce the amplitudes and frequencies of the vertical velocity gravity mode perturbations associated with the smallest waves. For a wavelength of 20 km, the bottom of the mesobeta scale, the QNH1 model reduces amplitude by 50%, QNH2 by over 80%, and QNH3 by over 90%. Each of the models reduce the amplitude and frequencies of the gravity waves by increasing amounts as the wavelengths get shorter. The QNH2 model, which is designed for the mesobeta scale, has approximately a 25% amplitude and frequency reduction for an $O(100\text{ km})$ wave, increasing as the wavelength approaches the lower end.

An important effect of the quasi-nonhydrostatic constant can be understood by examination of Fig. 7. The constant can be used to selectively limit the small-scale gravity wave modes that cause instability and errors, while not affecting the larger scale modes that are important in the prediction. By definition, a fully nonhydrostatic model has no amplitude or frequency reduction of this type. This is related to the concept of roughness in the initial state and forcing that has been discussed recently by Browning and Kreiss (1994a). The initial-state perturbations of small horizontal

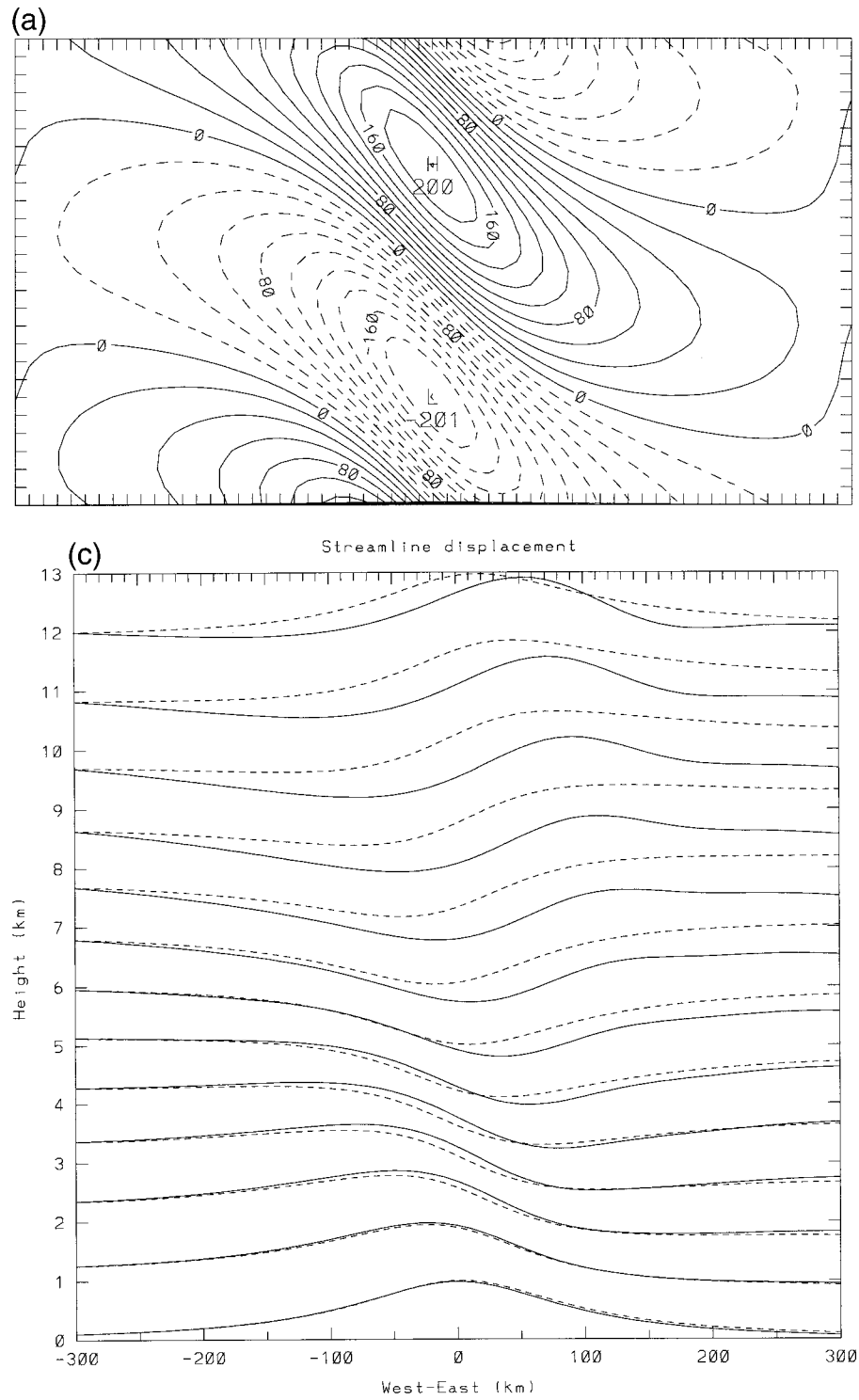


FIG. 6. Solution of Long's (1953) equation for vertically propagating, hydrostatic mountain waves. (a) Analytic solution of vertical velocity ($\text{m s}^{-1} \times 1000$) for $U = 20 \text{ m s}^{-1}$, height of the mountain of 100 m, and size of the bell-shaped mountain, " a " = 100 km. The domain of simulation is 640 km in the horizontal and 13 km in the vertical. (b) Same as (a), except solution is from a QNH2 model. The model solution is surprisingly good, considering that waves of wavelength less than 60 km are artificially ducted. Streamlines (exaggerated in the vertical by a factor of 10) of the analytic

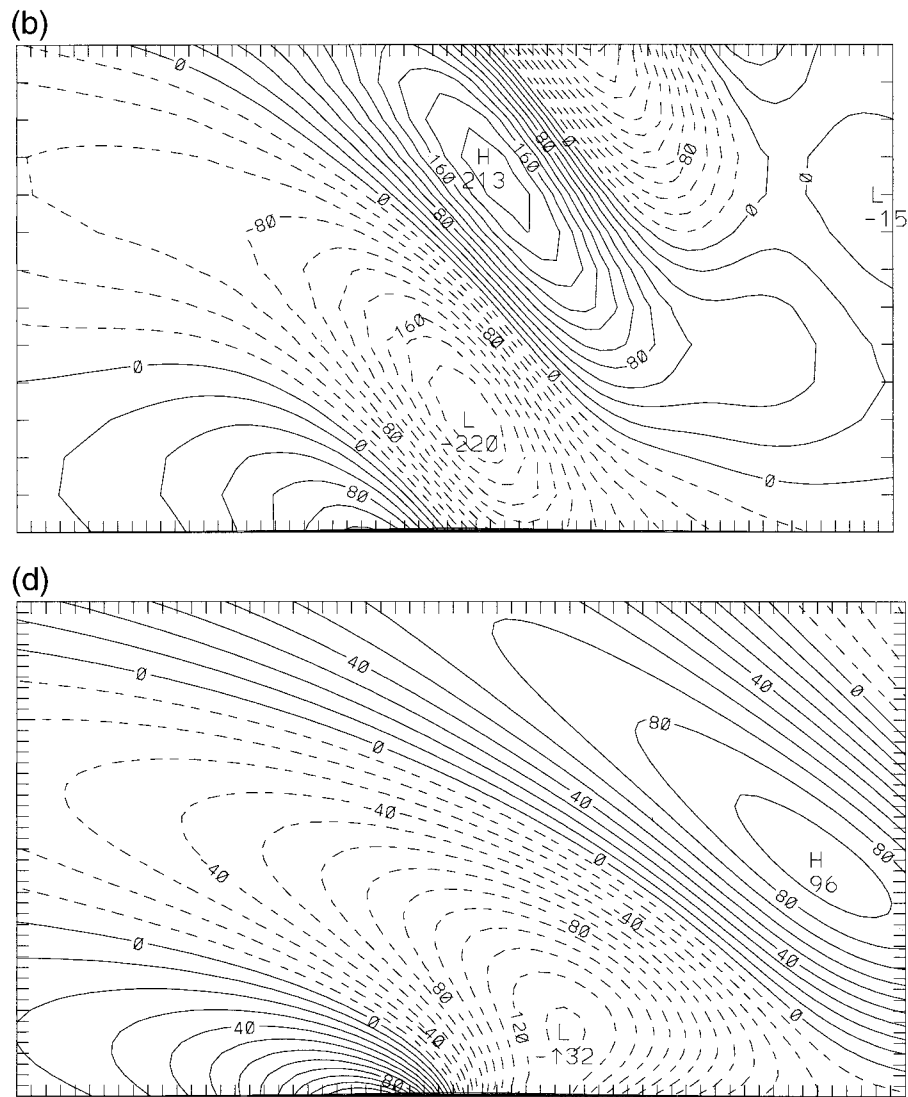


FIG. 6. (Continued) solution (solid lines) and the QNH2 solution (dashed lines). The flow is reasonably accurate in the low levels but departs significantly in the upper levels. (d) Same as (a), except from a QNH3 model. Comparing with the analytic vertical velocity in (a), it is clear that the magnitude of the centers are 50% too small, and they are far out of phase. This shows that when $\alpha = 10^{-3}$, terrain-forced, vertically propagating waves of horizontal scale $O(100 \text{ km})$ will be improperly handled by the model.

wavelength and deep vertical extent are in some sense rough, and the effect of the quasi-nonhydrostatic constant is to limit their amplitude and frequencies. The bounded derivative initialization, the enforcement of smoothness in the forcing and the constant, α , all work to keep the the amount of energy in the fast modes under control and well behaved. Browning and Kreiss (1986, 1994a, 1997) fully explore these concepts. We refer to the small-scale forcing as error modes; if explicit calculation of these modes is desired the horizontal and vertical resolution of the model can be increased, while making the quasi-nonhydrostatic parameter appropriately smaller.

We continue the discussion of the effect of the quasi-nonhydrostatic constant on gravity waves with an example of a perturbation of an initial field in a layer of medium depth. We let the vertical wavelength, L_z , be equal to 4 km, and investigate how a quasi-nonhydrostatic constant of $\alpha = 10^{-2}$ affects gravity waves of horizontal wavelengths at both ends of the mesobeta scale, $L_x = 20 \text{ km}$ and $L_x = 200 \text{ km}$. Perturbations of this scale are common due to radiation and latent heating effects. The result of the linear analysis of appendix B can be written as

$$\hat{w}(t) = \delta\theta\bar{\theta}^{-1}N\beta \cos(|N\beta|t),$$

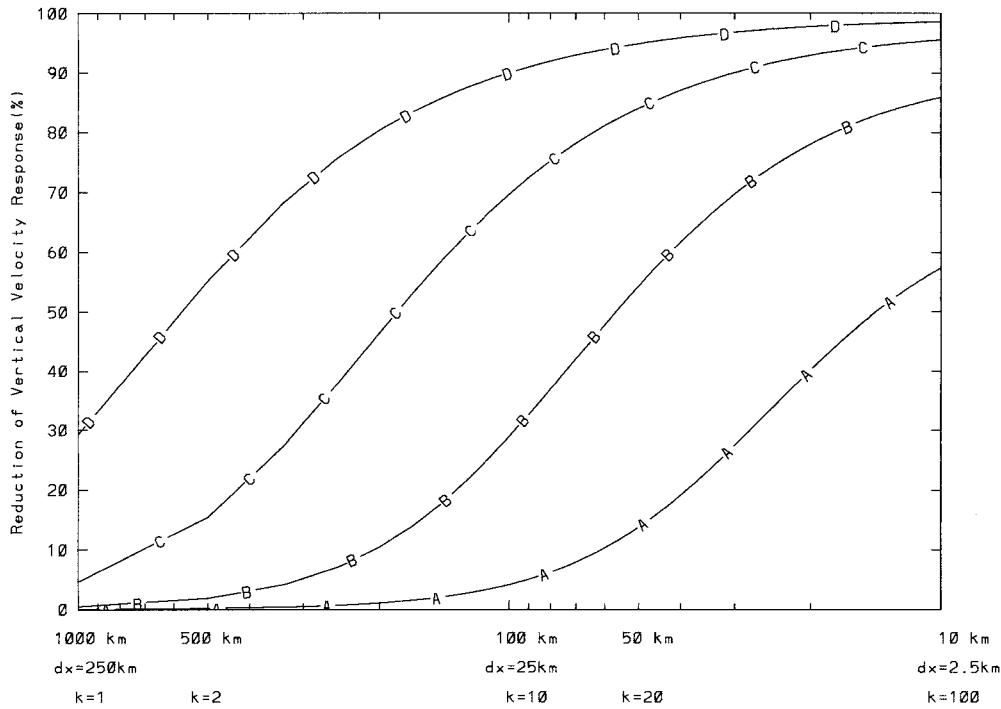


FIG. 7. Reduction of vertical velocity in response to perturbations in initial state, or to impulses in heating. It is assumed that the impulse is approximately through the scale height of the atmosphere (10 km). The QNH1 model is shown as A-A-A, QNH2 is B-B-B, QNH3 is C-C-C, and QNH4 is D-D-D. Examining line B-B-B, it is clear that a QNH model with $\alpha = 10^{-2}$ reduces responses to waves less than 100 km in wavelength quite substantially, with smaller reductions for larger waves. Thus, a main effect of the quasi-nonhydrostatic parameter is to decrease the vertical velocity in response to unbalanced initial conditions and to impulses in forcing.

where

$$\beta = \frac{1}{\alpha^{-1} + (L_x/L_z)^2}$$

We assume that the initial perturbation $\delta\theta$ has an amplitude of 3 K, the buoyancy frequency is $N = 10^{-2}$, s^{-1} , the stability parameter is $\tilde{\theta} = 10^{-5}$, and we calculate the amplitude and period of the response. The result is shown in Table 2. At the upper end of the mesobeta scale, $L_x = 200$ km, there is only a small

TABLE 2. Effect of the quasi-nonhydrostatic constant on gravity mode vertical response to initial-state perturbation. The result is from a linear analysis with an initial potential temperature perturbation of 3 K, and a vertical wavelength of 4 km.

Horizontal wavelength	$\alpha = 1$	$\alpha = 0.01$
Vertical velocity amplitude		
$L_x = 200$ km	20 cm s^{-1}	19.6 cm s^{-1}
$L_x = 20$ km	1.96 m s^{-1}	0.89 m s^{-1}
Period of gravity wave		
$L_x = 200$ km	5000 s	5100 s
$L_x = 20$ km	510 s	1118 s

change in the amplitude and period of the gravity wave. At the smaller end of the mesobeta scale, $L_x = 20$ km, there is a very substantial decrease of the amplitude, from nearly 2 m s^{-1} to less than 1 m s^{-1} , and increase of the period from about 10 to 20 min. The choice of α to correspond to an aspect ratio of 0.1 results in preserving the gravity wave response to perturbations of larger scale and decreasing the response to smaller waves.

The linear analysis of the gravity mode vertical velocity response to impulses in heating is detailed in appendix C. A solution of the inhomogenous system with a short heating impulse is somewhat more complex than the initial temperature perturbation analysis, but the result is similar:

$$\hat{w}_g(t) = \tilde{\theta}^{-1} H |\omega_g| T_0 r e^{i\nu t}$$

where r is the norm of $[e^{\omega_g t} - i \cos(|\omega_g|t)]$

$$r = \sqrt{1 + 2 \sin(|\omega_g|t) \cos(|\omega_g|t) + \cos^2(|\omega_g|t)}$$

$$\nu = \arccos\left(\frac{\cos(|\omega_g|t)}{r}\right)$$

In the equations above, H is the magnitude of the heating impulse, T_0 is the length of the impulse in time,

and ω_g is the gravity mode frequency that has been discussed earlier. It is clear that the response to heating impulses of the gravity mode of the vertical velocity is decreased with a functional dependence similar to that shown in Fig. 7. The amplitude and frequency are both reduced, with the smallest-scale perturbations being decreased the most.

An experiment was conducted to illustrate the effect of a rough heating impulse in the QNH model. The impulse was Gaussian in time and space, with rise and fall times of 1 min, and an e -fold radius of 40 km in the horizontal and 4 km in the vertical. Figure 8a shows the vertical velocity response to the impulse in a fully nonhydrostatic version of the model, and Fig. 8b shows the response when $\alpha = 10^{-2}$. The large-amplitude wave in both runs is the forced wave response. Note that the amplitude of the response for the QNH2 run is reduced and that the frequency of the response is also significantly reduced, as would be expected from the linear analysis of appendix C. The fully nonhydrostatic run has a much stronger high-frequency component, which are gravity waves. Figure 8 is the best illustration of the advantages and disadvantages of the quasi-nonhydrostatic model. The advantage—stability—is evident in the great reduction of small-scale gravity wave energy. The disadvantage—slower hydrostatic adjustment—is evident in the damped oscillation seen over several hours in Fig. 8b.

It may seem inconsistent to emphasize the accuracy of a QNH2 model gravity waves in the section on free gravity waves, while emphasizing the reduction of unwanted gravity wave energy in this section; however, the two differ in their vertical length scale. It has been shown that the model is quite accurate for free gravity waves with typical scale heights of about a kilometer, while at the same time it decreases response to deep perturbations of the order of 10 km in the vertical.

4. Conclusions

This paper has presented a discussion of the theory of quasi-nonhydrostatic models. It has been argued that such models should be superior to hydrostatic models, which are ill posed for limited domains and unstable for small-scale moist convection. It is further argued that when the proper quasi-nonhydrostatic parameter is used, these models should be more stable and resistant to growth of errors in small-scale fast modes than fully nonhydrostatic models. Most significantly, it has been shown that the effect of the quasi-nonhydrostatic parameter is to decrease the frequency and amplitude of the small-scale gravity-mode response to forcing. Their ability to make better weather predictions than fully nonhydrostatic models is yet to be determined. Their stability should allow model integrations with less dissipation and therefore less negative impact in structures of interest such as Rossby waves. However, as the quasi-

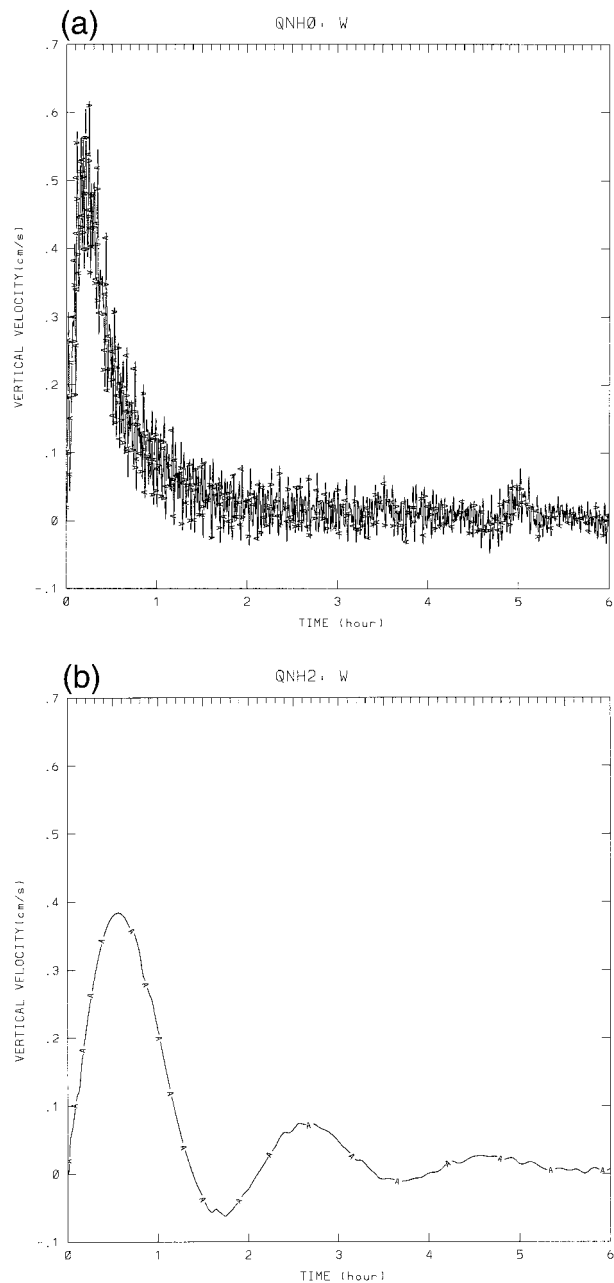


FIG. 8. Response of vertical velocity (cm s^{-1}) to an initial 1-min impulse in heating. The impulse is Gaussian in time and space, with an e -fold radius of 40 km in the horizontal, and 4 km in the vertical, and a peak value of 1 J kg^{-1} . (a) In the fully nonhydrostatic model, there is a sharp rise and fall within the first hour of the gravity wave component of the response. Superposed on the gravity wave is a high-frequency acoustic wave that continues through time. (b) When $\alpha = 10^{-2}$, the frequency of the gravity wave is slowed down so that it exists while damping for several hours. The acoustic response is greatly decreased. Notice that the amplitude of the gravity mode response is also decreased, reaching over 0.6 cm s^{-1} in the fully nonhydrostatic run, but limited to less than 0.4 cm s^{-1} in the QNH2 run. The decrease of the amplitude and frequency of high-frequency waves clearly evident in comparing these two graphs reveals an important effect of the quasi-nonhydrostatic parameter.

nonhydrostatic parameter becomes smaller, it slows down hydrostatic adjustment. The trade-off between these two effects is an important issue that can only be evaluated by extensive comparisons of full physics versions of both types of model making real weather predictions.

Although we have referred to realizations of the quasi-nonhydrostatic model as “different” models, it is not difficult to convert from one (e.g., QNH2) to another (e.g., QNH3). The programs are written so that the quasi-nonhydrostatic parameter may be simply changed. A more challenging issue is to tailor the physics packages to the phenomena and scales of interest. The quasi-nonhydrostatic parameter allows the modeler to choose the phenomena of interest, and suppress explicit phenomena of smaller time- and space scales.

For mesoscale prediction, the theory indicates that a QNH3 model should be accurate for cloud and precipitation prediction throughout the mesoalpha scale, and well into the mesobeta scale, but will not handle small-scale terrain-forced gravity waves. It should have very smooth evolution of mesoscale features such as upslope precipitation, as is shown for the winter storm case presented in MacDonald et al. (2000). A QNH2 model can accommodate cloud and precipitation down to $O(10 \text{ km})$ and will give reasonably accurate prediction of terrain-forced gravity wave phenomena such as hydrostatic, nonrotating waves of scales of 100 km and larger. It should be better than a QNH3 model in its response to small-scale local forcing, such as those caused by surface inhomogeneities like land–water contrasts. Inertia–gravity waves with effects such as trapping and vertical energy propagation should be acceptably predicted with a QNH2 model. As predicted by the theory, our experience indicates that the QNH2 model is excellent for mesobeta-scale prediction of forced phenomena, such as sea breezes and small-scale terrain flow, as well as its design goal of smoothly evolving vertical velocity fields and precipitation.

It is concluded that the implementation of a quasi-nonhydrostatic mesoscale weather prediction model based on the theory of Browning and Kreiss (1986) is feasible and that such a model may have a number of advantages such as improved prediction of clouds and precipitation.

Acknowledgments. We would like to gratefully acknowledge that this effort would not have been possible without the ideas and many years of guidance provided by Gerald L. Browning.

APPENDIX A

Eigenanalysis for a Linearized Quasi-Nonhydrostatic System

In this appendix, we analyze a simplified form of the quasi-nonhydrostatic equation set to illustrate the char-

acteristics of Rossby, gravity, and acoustic waves for a linear system. It will be shown that the quasi-nonhydrostatic constant does not affect the Rossby waves but has an effect on the small-scale gravity waves and vertical sound waves, similar to that of Browning and Kreiss (1985). This analysis leads to an analysis of the effect of perturbations of initial state (appendix B) and in forcing (appendix C).

We start with a linearized, somewhat simplified version of Eqs. (1)–(5) that is presented in Eqs. (8)–(12). Note that two dynamic terms were dropped, which are lower order, from the w and p equations. These can be shown as small terms in a scale analysis, and so do not change the linear wave analysis. In addition, we drop the mean flow to simplify the wave analysis.

From section 2a, the eigenmatrix of a linearized QNH is

$$(\mathbf{A} - \omega \mathbf{I}) = \begin{pmatrix} -\omega & f & 0 & -ik\rho_0^{-1} & 0 \\ -f & -\omega & 0 & -il\rho_0^{-1} & 0 \\ 0 & 0 & -\omega & -im\alpha\rho_0^{-1} & \alpha g \\ -\gamma p_0 ik & -\gamma p_0 il & -\gamma p_0 im & -\omega & 0 \\ 0 & 0 & -\tilde{\theta} & 0 & -\omega \end{pmatrix}.$$

Setting its determinant to zero gives the characteristic equation

$$\omega^5 + [f^2 + \rho_0^{-1}\gamma p_0(k^2 + l^2) + \rho_0^{-1}\gamma p_0\alpha m^2 + \alpha N^2]\omega^3 + [f^2\alpha N^2 + \rho_0^{-1}\gamma p_0(k^2 + l^2)\alpha N^2 + \rho_0^{-1}\gamma p_0\alpha m^2 f^2]\omega = 0, \quad (\text{A1})$$

where $N^2 = g\tilde{\theta}$ is the square of the Brunt–Väisälä frequency. Solving this polynomial gives the eigenvalues as follows:

$$\omega_{\text{Rossby}} = 0 \quad (\text{A2})$$

$$\omega_{\text{gravity}\pm} = \pm \sqrt{\frac{-C_1 + \sqrt{C_1^2 - 4C_2}}{2}} \quad (\text{A3})$$

$$\omega_{\text{sound}\pm} = \pm \sqrt{\frac{-C_1 - \sqrt{C_1^2 - 4C_2}}{2}}, \quad (\text{A4})$$

where

$$C_1 = \rho_0^{-1}\gamma p_0(k^2 + l^2) + \rho_0^{-1}\gamma p_0\alpha m^2 + \alpha N^2 + f^2 \quad (\text{A5})$$

$$C_2 = f^2\alpha g\tilde{\theta} + \rho_0^{-1}\gamma p_0\alpha N^2(k^2 + l^2) + \rho_0^{-1}\gamma p_0\alpha m^2 f^2. \quad (\text{A6})$$

Expression C_1 can be interpreted as sum of the squares of each of three frequencies: the first term being the sound waves (modified in the vertical by α), the second term the buoyancy frequency (also multiplied by α), and the third term the Rossby wave frequency. It is clear from scaling considerations for the mesoscale that the

Coriolis term and the buoyancy term can be dropped from C_1 as well as C_2 . That is,

$$C_1 \approx \rho_0^{-1} \gamma p_0 (k^2 + l^2) + \rho_0^{-1} \gamma p_0 \alpha m^2 \quad (\text{A7})$$

$$C_2 \approx \rho_0^{-1} \gamma p_0 \alpha N^2 (k^2 + l^2). \quad (\text{A8})$$

It is obvious that $C_2 \ll C_1$ and then $\Delta = (4C_2)/C_1^2$ is small and

$$\begin{aligned} \omega_g &\equiv \sqrt{\frac{-C_1 + \sqrt{C_1^2 - 4C_2}}{2}} = \sqrt{\frac{-C_1 + C_1 \sqrt{1 - \Delta}}{2}} \\ &\approx \sqrt{\frac{-C_1 + C_1 \left(1 - \frac{\Delta}{2}\right)}{2}} = i \sqrt{\frac{C_1 \Delta}{4}} = i \sqrt{\frac{C_2}{C_1}} \\ &\approx i \sqrt{\frac{N^2 (k^2 + l^2)}{\alpha^{-1} (k^2 + l^2) + m^2}} \end{aligned} \quad (\text{A9})$$

$$\begin{aligned} \omega_s &\equiv \sqrt{\frac{-C_1 - \sqrt{C_1^2 - 4C_2}}{2}} \approx i \sqrt{C_1} \\ &= [\rho_0^{-1} \gamma p_0 (k^2 + l^2 + \alpha m^2)]^{1/2}. \end{aligned} \quad (\text{A10})$$

To obtain the eigenvectors, we solve the following system by setting one component of the eigenvector to 1, and computing the remaining components:

$$(\mathbf{A} - \omega \mathbf{I}) \hat{V} = 0,$$

where $\hat{V}^T = (\hat{u}, \hat{v}, \hat{w}, \hat{p}, \hat{\theta})$. Here we set $\hat{\theta} = 1$.

$$\begin{pmatrix} \hat{u} \\ \hat{v} \\ \hat{w} \\ \hat{p} \\ \hat{\theta} \end{pmatrix} = \begin{pmatrix} -\omega^{-1} i \rho_0^{-1} k \hat{p} \\ -\omega^{-1} i \rho_0^{-1} l \hat{p} \\ -\tilde{\theta}^{-1} \omega \\ \hat{p}_j \\ 1 \end{pmatrix},$$

where

$$\begin{aligned} \hat{p}_j &= (i \rho_0^{-1} \alpha m^{-1} (\alpha g + \tilde{\theta}^{-1} \omega^2)) \\ &= (i \rho_0^{-1} m)^{-1} (g + \tilde{\theta}^{-1} \alpha^{-1} \omega^2). \end{aligned} \quad (\text{A11})$$

For the Rossby wave, we can easily show that $(\hat{u}, \hat{v}, \hat{w}, \hat{p}, \hat{\theta}) = (l, -k, 0, 0, 0)$ is its eigenvector.

Define the eigenvector matrix \mathbf{X} as

$$\mathbf{X} = \begin{pmatrix} l & -\omega_2^{-1} i \rho_0^{-1} k \hat{p}_2 & -\omega_3^{-1} i \rho_0^{-1} k \hat{p}_3 & -\omega_4^{-1} i \rho_0^{-1} k \hat{p}_4 & -\omega_5^{-1} i \rho_0^{-1} k \hat{p}_5 \\ -k & -\omega_2^{-1} i \rho_0^{-1} l \hat{p}_2 & -\omega_3^{-1} i \rho_0^{-1} l \hat{p}_3 & -\omega_4^{-1} i \rho_0^{-1} l \hat{p}_4 & -\omega_5^{-1} i \rho_0^{-1} l \hat{p}_5 \\ 0 & -\tilde{\theta}^{-1} \omega_2 & -\tilde{\theta}^{-1} \omega_3 & -\tilde{\theta}^{-1} \omega_4 & -\tilde{\theta}^{-1} \omega_5 \\ 0 & \hat{p}_2 & \hat{p}_3 & \hat{p}_4 & \hat{p}_5 \\ 0 & 1 & 1 & 1 & 1 \end{pmatrix}.$$

Since $\omega_2 = -\omega_4$, $\omega_3 = -\omega_5$ and $\hat{p}_2 = \hat{p}_4$, $\hat{p}_3 = \hat{p}_5$,

$$\mathbf{X} = \begin{pmatrix} l & -\omega_2^{-1} i \rho_0^{-1} k \hat{p}_2 & -\omega_3^{-1} i \rho_0^{-1} k \hat{p}_3 & \omega_2^{-1} i \rho_0^{-1} k \hat{p}_2 & \omega_3^{-1} i \rho_0^{-1} k \hat{p}_3 \\ -k & -\omega_2^{-1} i \rho_0^{-1} l \hat{p}_2 & -\omega_3^{-1} i \rho_0^{-1} l \hat{p}_3 & \omega_2^{-1} i \rho_0^{-1} l \hat{p}_2 & \omega_3^{-1} i \rho_0^{-1} l \hat{p}_3 \\ 0 & -\tilde{\theta}^{-1} \omega_2 & -\tilde{\theta}^{-1} \omega_3 & \tilde{\theta}^{-1} \omega_2 & \tilde{\theta}^{-1} \omega_3 \\ 0 & \hat{p}_2 & \hat{p}_3 & \hat{p}_4 & \hat{p}_3 \\ 0 & 1 & 1 & 1 & 1 \end{pmatrix}.$$

The general solution of the system is

$$Y = \sum_{j=1}^5 \eta_j e^{\omega_j t} X_j, \quad (\text{A12})$$

where $\omega_1 = \omega_{\text{Rossby}}$, $\omega_2 = \omega_g$, $\omega_4 = -\omega_g$ and $\omega_3 = \omega_s$, $\omega_5 = -\omega_s$.

APPENDIX B

Particular Solution for Perturbation in Initial Potential Temperature

In this appendix, we derive a particular solution that has a perturbation of potential temperature in the

initial condition. Assume $\delta\theta$ is the perturbation at the initial time. From the general solution of the system, we have

$$Y(0) = \sum_{j=1}^5 \eta_j X_j = XV$$

where $V = (\eta_1, \eta_2, \eta_3, \eta_4, \eta_5)$. If we choose $Y(0) = (0, 0, 0, 0, \delta\theta)$,

$$XV = (0, 0, 0, 0, \delta\theta).$$

To solve this system, we perform Gaussian elimination on the augmented system:

$$\begin{pmatrix} l & -\omega_2^{-1}i\rho_0^{-1}k\hat{p}_2 & -\omega_3^{-1}i\rho_0^{-1}k\hat{p}_3 & \omega_2^{-1}i\rho_0^{-1}k\hat{p}_2 & \omega_3^{-1}i\rho_0^{-1}k\hat{p}_3 & 0 \\ -k & -\omega_2^{-1}i\rho_0^{-1}l\hat{p}_2 & -\omega_3^{-1}i\rho_0^{-1}l\hat{p}_3 & \omega_2^{-1}i\rho_0^{-1}l\hat{p}_2 & \omega_3^{-1}i\rho_0^{-1}l\hat{p}_3 & 0 \\ 0 & -\tilde{\theta}^{-1}\omega_2 & -\tilde{\theta}^{-1}\omega_3 & \tilde{\theta}^{-1}\omega_2 & \tilde{\theta}^{-1}\omega_3 & 0 \\ 0 & \hat{p}_2 & \hat{p}_3 & \hat{p}_2 & \hat{p}_3 & 0 \\ 0 & 1 & 1 & 1 & 1 & \delta\theta \end{pmatrix}$$

and obtain the following matrix

$$\begin{pmatrix} l & -\omega_2^{-1}i\rho_0^{-1}k\hat{p}_2 & -\omega_3^{-1}i\rho_0^{-1}k\hat{p}_3 & \omega_2^{-1}i\rho_0^{-1}k\hat{p}_2 & \omega_3^{-1}i\rho_0^{-1}k\hat{p}_3 & 0 \\ 0 & 0 & d_1 & 0 & d_2 & \delta\theta\omega_2^{-1}\hat{p}_2 \\ 0 & 0 & \omega_3 - \frac{\omega_2^2\hat{p}_3}{\omega_3\hat{p}_2} & 0 & -\omega_3 + \frac{\omega_2^2\hat{p}_3}{\omega_3\hat{p}_2} & 0 \\ 0 & 0 & \hat{p}_3\left(1 - \frac{\omega_2}{\omega_3}\right) & 2\hat{p}_2 & \hat{p}_3\left(1 + \frac{\omega_2}{\omega_3}\right) & 0 \\ 0 & 1 & 1 & 1 & 1 & \delta\theta \end{pmatrix},$$

where

$$d_1 = -\omega_3^{-1}\hat{p}_3 + \omega_2^{-1}\hat{p}_2 - \omega_2^{-1}\hat{p}_3\left(1 - \frac{\omega_2}{\omega_3}\right)$$

$$d_2 = \omega_3^{-1}\hat{p}_3 + \omega_2^{-1}\hat{p}_2 - \omega_2^{-1}\hat{p}_3\left(1 + \frac{\omega_2}{\omega_3}\right).$$

The third row implies that $\eta_3 = \eta_5$ and then the second row gives

$$2\omega_2^{-1}(\hat{p}_2 - \hat{p}_3)\eta_3 = \delta\theta\omega_2^{-1}\hat{p}_2 \quad \eta_3 = \frac{\delta\theta}{2} \frac{\hat{p}_2}{\hat{p}_2 - \hat{p}_3}.$$

And from the fourth row,

$$2\hat{p}_2\eta_4 + 2\hat{p}_3\eta_3 = 0,$$

which implies

$$\eta_4 = -\frac{\hat{p}_3}{\hat{p}_2}\eta_3 = -\frac{\hat{p}_3}{\hat{p}_2} \frac{\delta\theta}{2} \frac{\hat{p}_2}{\hat{p}_2 - \hat{p}_3} = -\frac{\delta\theta}{2} \frac{\hat{p}_3}{\hat{p}_2 - \hat{p}_3}.$$

By the definition of \hat{p}_j , we know that $\hat{p}_2 \ll \hat{p}_3$ and $\hat{p}_2/\hat{p}_2 - \hat{p}_3 \approx -1$ and therefore

$$\eta_3 \approx -\frac{\delta\theta}{2} \frac{\hat{p}_2}{\hat{p}_3} \quad \eta_4 \approx \frac{\delta\theta}{2}.$$

From the fifth row,

$$\eta_2 = \delta\theta - 2\eta_3 - \eta_4 \approx \frac{\delta\theta}{2}.$$

Consider the gravity mode of the w component

$$\begin{aligned} \hat{w}_g(t) &= -\tilde{\theta}^{-1}\omega_2(\eta_2e^{\omega_2 t} + \eta_4e^{-\omega_2 t}) \\ &\approx \tilde{\theta}^{-1}\omega_2 \frac{\delta\theta}{2}(e^{\omega_2 t} + e^{-\omega_2 t}) = \tilde{\theta}^{-1}\omega_g\delta\theta \cos(|\omega_g|t). \end{aligned}$$

This is the main result from the particular solution of

the response of the gravity mode of vertical velocity to a perturbation in the initial potential temperature; it shows how both the amplitude and frequency are affected by the modified gravity wave frequency:

$$\omega_g = i \sqrt{\frac{N^2(k^2 + l^2)}{\alpha^{-1}(k^2 + l^2) + m^2}}.$$

By Parseval's relation, we know that the same conclusion concerning the amplitude of the gravity wave in the \hat{w} component also holds in physical space.

APPENDIX C

Solution of Inhomogeneous System Response to Heating Impulse

We now want to solve the inhomogeneous, linear quasi-nonhydrostatic equation system to determine the response of the system to an impulse in heating. Assume H is the heating function that is a function of time, $\mathcal{H} = \mathcal{H}(t)$. From ordinary differential equation theory, we assume $\eta_j = \eta_j(t)$.

Taking η_j as a function of t and putting the general solution (28) into the system

$$\frac{\partial Y}{\partial t} = AY + \mathcal{F},$$

where $\mathcal{F} = (0, 0, 0, 0, \mathcal{H})^T$, and we have

$$\sum_{j=1}^5 \eta'_j e^{\omega_j t} X_j + \sum_{j=1}^5 \eta_j \omega_j e^{\omega_j t} X_j = AY + \mathcal{F}$$

$$\sum_{j=1}^5 \eta'_j e^{\omega_j t} X_j + \sum_{j=1}^5 \eta_j e^{\omega_j t} AX_j = AY + \mathcal{F}$$

$$\sum_{j=1}^5 \eta'_j e^{\omega_j t} X_j + AY = AY + \mathcal{F}.$$

This implies

$$X \begin{pmatrix} \eta'_1 e^{\omega_1 t} \\ \eta'_2 e^{\omega_2 t} \\ \eta'_3 e^{\omega_3 t} \\ \eta'_4 e^{\omega_4 t} \\ \eta'_5 e^{\omega_5 t} \end{pmatrix} = \mathcal{F}$$

and then

$$XV = \mathcal{F},$$

where $V = (v_1, v_2, v_3, v_4, v_5)^T = (\eta'_1 e^{\omega_1 t}, \eta'_2 e^{\omega_2 t}, \eta'_3 e^{\omega_3 t}, \eta'_4 e^{\omega_4 t}, \eta'_5 e^{\omega_5 t})$. Using the result of the Gaussian elimination in appendix B on the augmented system $(X|\mathcal{F})$,

$$\left(\begin{array}{cccccc} l & -\omega_2^{-1} i \rho_0^{-1} k \hat{p}_2 & -\omega_3^{-1} i \rho_0^{-1} k \hat{p}_3 & \omega_2^{-1} i \rho_0^{-1} k \hat{p}_2 & \omega_3^{-1} i \rho_0^{-1} k \hat{p}_3 & 0 \\ 0 & 0 & d_1 & 0 & d_2 & \mathcal{H} \omega_2^{-1} \hat{p}_2 \\ 0 & 0 & \omega_3 - \frac{\omega_2^2 \hat{p}_3}{\omega_3 \hat{p}_2} & 0 & -\omega_3 + \frac{\omega_2^2 \hat{p}_3}{\omega_3 \hat{p}_2} & 0 \\ 0 & 0 & \hat{p}_3 \left(1 - \frac{\omega_2}{\omega_3} \right) & 2\hat{p}_2 & \hat{p}_3 \left(1 + \frac{\omega_2}{\omega_3} \right) & 0 \\ 0 & 1 & 1 & 1 & 1 & \mathcal{H} \end{array} \right).$$

Similar to appendix B by simply replacing $\delta\theta$ by \mathcal{H} , we have

$$v_2 \approx \frac{\mathcal{H}}{2} \quad v_3 \approx \frac{\mathcal{H}}{2}$$

or by defining

$$\hat{H}_i = \int_0^t \mathcal{H} e^{-\omega_i \zeta} d\zeta,$$

we have equations for η_2 and η_4

$$\eta_2(t) - \eta_2(0) \approx \frac{\hat{H}_2}{2} \quad \eta_4(t) - \eta_4(0) \approx \frac{\hat{H}_4}{2}.$$

Consider the gravity wave mode of the w component:

$$\begin{aligned} \hat{w}_g(t) &= -\tilde{\theta}^{-1} \omega_2 (\eta_2(t) e^{\omega_2 t} + \eta_4(t) e^{-\omega_2 t}) \\ &= -\tilde{\theta}^{-1} \omega_2 \left\{ \eta_2(0) e^{\omega_2 t} + \eta_4(0) e^{-\omega_2 t} \right. \\ &\quad \left. + \left[\left(1 - \frac{\hat{p}_2}{\hat{p}_2 - \hat{p}_3} - \frac{\hat{p}_3}{2(\hat{p}_2 - \hat{p}_3)} \right) \hat{H}_2 e^{\omega_2 t} \right. \right. \\ &\quad \left. \left. - \frac{\hat{p}_3}{2(\hat{p}_2 - \hat{p}_3)} \hat{H}_4 e^{-\omega_2 t} \right] \right\}. \end{aligned}$$

Consider a case with initial condition $Y(0) = 0$ that implies $\eta_j(0) = 0$ for $j = 1, \dots, 5$. That is, the gravity mode of the \hat{w} component is

$$\hat{w}_g(t) = -\tilde{\theta}^{-1} \omega_2 \frac{\hat{p}_3}{\hat{p}_2 - \hat{p}_3} \left[\hat{H}_2 e^{\omega_2 t} - \frac{1}{2} (\hat{H}_2 e^{\omega_2 t} + \hat{H}_4 e^{-\omega_2 t}) \right].$$

Now consider a case where \mathcal{H} is an impulse function, that is,

$$\mathcal{H} = H(t - T_0)_+ = \begin{cases} 0 & t > T_0 \\ H & t \leq T_0, \end{cases}$$

where H is a constant that is the amplitude of the impulse. An example of such a heating impulse is the initial 1 min of heating that was described in section 3f and shown in Fig. 8. We then get

$$e^{\omega_2 t} \hat{H}_2 = e^{\omega_2 t} \int_0^t \mathcal{H} e^{-\omega_2 \zeta} d\zeta$$

$$\begin{aligned} &= \begin{cases} H e^{\omega_2 t} \int_0^t e^{-\omega_2 \zeta} d\zeta & t \leq T_0 \\ H e^{\omega_2 t} \int_0^{T_0} e^{-\omega_2 \zeta} d\zeta & t > T_0 \end{cases} \\ &= \begin{cases} -H \frac{e^{\omega_2 t}}{\omega_2} e^{-\omega_2 \zeta} \Big|_0^t & t \leq T_0 \\ -H \frac{e^{\omega_2 t}}{\omega_2} e^{-\omega_2 \zeta} \Big|_0^{T_0} & t > T_0 \end{cases} \\ &= \begin{cases} H \frac{e^{\omega_2 t}}{\omega_2} [1 - e^{-\omega_2 t}] & t \leq T_0 \\ H \frac{e^{\omega_2 t}}{\omega_2} [1 - e^{-\omega_2 T_0}] & t > T_0. \end{cases} \end{aligned}$$

Similarly, as $\omega_4 = -\omega_2$,

$$\begin{aligned}
 e^{\omega_4 t} \hat{H}_4 &= e^{-\omega_2 t} \hat{H}_4 = e^{-\omega_2 t} \int_0^t \mathcal{H} e^{\omega_2 \zeta} d\zeta \\
 &= \begin{cases} H e^{-\omega_2 t} \int_0^t e^{\omega_2 \zeta} d\zeta & t \leq T_0 \\ H e^{-\omega_2 t} \int_0^{T_0} e^{\omega_2 \zeta} d\zeta & t > T_0 \end{cases} \\
 &= \begin{cases} \frac{H}{\omega_2} [e^{\omega_2 t} - 1] & t \leq T_0 \\ \frac{H}{\omega_2} [e^{\omega_2 T_0} - 1] & t > T_0. \end{cases}
 \end{aligned}$$

Thus, as ω_2 is pure imaginary,

$$\begin{aligned}
 \hat{H}_2 e^{\omega_2 t} + \hat{H}_4 e^{\omega_4 t} &= \begin{cases} \frac{H}{\omega_2} [e^{\omega_2 t} - e^{-\omega_2 t}] & t \leq T_0 \\ \frac{H}{\omega_2} [e^{\omega_2 t} - e^{-\omega_2 t} - e^{\omega_2(t-T_0)} + e^{-\omega_2(t-T_0)}] & t > T_0 \end{cases} \\
 &= \begin{cases} \frac{2iH}{\omega_2} \sin(|\omega_2|t) & t \leq T_0 \\ \frac{2iH}{\omega_2} [\sin(|\omega_2|t) - \sin(|\omega_2|(t - T_0))] & t > T_0. \end{cases}
 \end{aligned}$$

The gravity mode of the \hat{w} component becomes

$$\hat{w}_g(t) = \begin{cases} \tilde{\theta}^{-1} H [e^{\omega_2 t} - 1 - i \sin(|\omega_2|t)] & t \leq T_0 \\ \tilde{\theta}^{-1} H [e^{\omega_2 t} - e^{\omega_2(t-T_0)} - i(\sin(|\omega_2|t) - \sin(|\omega_2|(t - T_0)))] & t > T_0. \end{cases}$$

Thus for a small T_0 ,

$$e^{\omega_2 t} - e^{\omega_2(t-T_0)} \approx |\omega_2| T_0 e^{\omega_2 t}$$

$$\sin(|\omega_2|t) - \sin(|\omega_2|(t - T_0)) \approx |\omega_2| T_0 \cos(|\omega_2|t)$$

and therefore, for $t > T_0$,

$$\begin{aligned}
 \hat{w}_g(t) &\approx \tilde{\theta}^{-1} H |\omega_2| T_0 [e^{\omega_2 t} - i \cos(|\omega_2|t)] \\
 &= \tilde{\theta}^{-1} H |\omega_2| T_0 r e^{i\nu},
 \end{aligned}$$

where r is the norm of $[e^{\omega_2 t} - i \cos(|\omega_2|t)]$

$$r = \sqrt{1 + 2 \sin(|\omega_2|t) \cos(|\omega_2|t) + \cos^2(|\omega_2|t)}$$

$$\nu = \arccos\left(\frac{\cos(|\omega_2|t)}{r}\right).$$

That is, the magnitude of $\hat{w}_g(t)$ is proportional to α if the duration of heating is for a fairly short time. Although this was done for an initial impulse of heating, the generalization to an impulse of heating at any time during the integration is straightforward.

By Parseval's relation, we know the amplitude of the \hat{w} component of the gravity waves in physical space are also reduced as long as T_0 is small.

The results of the particular solution for perturbation of potential temperature at the initial time and the inhomogeneous solution for an impulse of heating during the model integration are similar. They both show that the effect of the quasi-nonhydrostatic constant, α , is to decrease both the frequency and amplitude of the gravity mode vertical velocity response. The effect is largest for deep waves of small horizontal extent.

REFERENCES

Black, T. L., Z. I. Janjić, and J. H. Ward, 1990: Heavy precipitation forecasts from NMC's Eta Model. Preprints, *16th Conf. on Severe Local Storms and Conf. on Atmospheric Electricity*, Kanawanski Park, AB, Canada, Amer. Meteor. Soc., J1-J4.

Browning, G. L., and H.-O. Kreiss, 1985: Numerical problems connected with weather prediction. *Progress in Scientific Computing*, E. M. Murman and S. S. Abarbanel, Eds. Vol. 6, Birkhauser, 377-394.

—, and —, 1986: Scaling and computation of smooth atmospheric motions. *Tellus*, **38A**, 295-313.

—, and A. E. MacDonald, 1993: Incorporating topography into the multiscale systems for the atmosphere and oceans. *Dyn. Atmos. Oceans*, **18**, 119-149.

—, and H.-O. Kreiss, 1994a: The impact of rough forcing on systems with multiple time scales. *J. Atmos. Sci.*, **51**, 369-383.

—, and —, 1994b: Splitting methods for problems of different timescales. *Mon. Wea. Rev.*, **122**, 2614-2622.

—, and —, 1997: The role of gravity waves in slowly varying in time mesoscale motions. *J. Atmos. Sci.*, **54**, 1166-1184.

—, A. Kasahara, and H.-O. Kreiss, 1980: Initialization of the primitive equations by the bounded derivative method. *J. Atmos. Sci.*, **37**, 1424-1436.

—, J. J. Hack, and P. N. Swartztrauber, 1989: A comparison of three numerical methods for solving differential equations on a sphere. *Mon. Wea. Rev.*, **117**, 1058-1075.

Gill, A. E., 1982: *Atmosphere-Ocean Dynamics*. Academic Press, 662 pp.

Klemp, J. B., and D. K. Lilly, 1978: Numerical simulation of hydrostatic mountain waves. *J. Atmos. Sci.*, **35**, 78-107.

Kreiss, H.-O., 1970: Initial boundary value problems for hyperbolic equations. *Comm. Pure Appl. Math.*, **33**, 277-298.

—, 1980: Problems with different time scales for partial differential equations. *Comm. Pure Appl. Math.*, **33**, 399-440.

—, and J. Lorenz, 1989: *Initial-Boundary Value Problems and the Navier-Stokes Equations*. Academic Press, 402 pp.

Lee, J. L., and A. E. MacDonald, 2000: QNH: Mesoscale bounded

- derivative initialization and winter storm test over complex terrain. *Mon. Wea. Rev.*, **128**, 1037–1051.
- Long, R. R., 1953: Some aspects of the flow of stratified fluids. I. A theoretical investigation. *Tellus*, **5**, 42–58.
- MacDonald, A. E., J. L. Lee, and S. Sun, 2000: QNH: Design and test of a quasi-nonhydrostatic model for mesoscale weather prediction. *Mon. Wea. Rev.*, **128**, 1016–1036.
- Olinger, J., and A. Sundstrom, 1978: Theoretical and practical aspects of some initial value problems in fluid dynamics. *SIAM, J. Appl. Math.*, **35**, 419–446.
- Orlanski, I., 1975: A rational subdivision of scales for atmospheric processes. *Bull. Amer. Meteor. Soc.*, **56**, 527–530.
- , 1981: The quasi-hydrostatic approximation. *J. Atmos. Sci.*, **38**, 572–582.
- Pielke, R. A., 1984: *Mesoscale Meteorological Modeling*. Academic Press, 612 pp.
- Skamarock, W. C., and J. B. Klemp, 1994: Efficiency and accuracy of the Klemp–Wilhelmson time-splitting technique. *Mon. Wea. Rev.*, **122**, 2623–2630.
- Smith, R. B., 1980: Linear theory of stratified hydrostatic flow past an isolated mountain. *Tellus*, **32**, 348–364.